Chapter 1

Introductory Chapter: Metrology

Anil Akdogan

Additional information is available at the end of the chapter

http://dx.doi.org/10.5772/intechopen.75541

1. Introduction

Metrology, the science of measurement, is crucial for manufacturing technologies. Since manufacturing has made huge leaps depending on the improvements in metrology, the book reflects recent developments in metrology in detail. This book focuses on dimensional and geometric measurements as well as technical testing and quality control applications in industry. It also intends the fundamentals of metrology concerning the related standards and systems of units. In addition, the book considers the calibration of measurement instruments and measurement uncertainties as the basic requirements of the related quality standards. Furthermore, it mentions the trends in micro and nanometrology and microscopic examinations. Topics covered in this book are of course not limited to them. The readers can find chapters about Metrology in a wide frame.

Physical properties such as length, weight, and temperature are determined by comparison with known quantities. In addition, measurement techniques are available in all engineering disciplines and allow for the creation and operation of all other scientific branches. In particular, measurement techniques are required at all levels of laboratory works. In fact, we practically measure many things: the weight of our body, the volume of our fuel oil, the temperature of the house, the noise at the factory, the distance between two points, etc. In addition to having an important place in our daily life, the measurement technique is the basis of almost all science branches such as Physics, Chemistry, and Biology. Measurement techniques are used to solve technical problems at all science branches. Theoretical hypotheses are supported by proving correctness by means of measurement technique by making necessary experiments and observations.

Metrology is the science of measurement. It covers all the practical and theoretical topics based on measurement, regardless of accuracy level and application area [1]. Measurement processes, measurement methods and procedures, instrumentation, calibration, determination of

measurement systems, verification, measurement accuracy, measurement precision, measurement error, data acquisition, evaluation of measurement results, the formation of statistical evaluations, and quality determinations are the main subjects of metrology.

The recognition that a measurement made by an industrial device is recognized worldwide and is the same as any other measurement made possible by achieving the highest precision basic measurement standard with a measurement reference chain. By fulfilling this, it is ensured that all the measurements carried out are accepted nationally and/or internationally. As a result, the calibration and verification processes have gained a great deal of importance. Calibration is a process of establishing a link between the values indicated by a measuring instrument or measuring system under certain conditions and the values obtained by a measuring instrument and corresponding values of corresponding measured values. With calibration, the measurement of a less precise measuring instrument or standard is carried out using an accepted standard of accuracy [2]. National metrology institutes are operating at the highest level, linked to the system by reference chain. These institutions are also linked to the Bureau International des Poids et Measure (BIPM) in central Paris in order to ensure that the measurements are internationally recognizable in a hierarchical structure. In the process of industrialization which started with serial production, it has become very important to establish a whole by combining the parts produced in different places, initiate specialization forms in the subsidiary industry and production, and make the measurements internationally recognizable.

The reliability of measuring instruments has increased at the same rate as the widespread use of microelectronics. Nowadays, measurement techniques are required to meet demands for faster, more accurate, and more flexible measurements. The documentation of measurement results is equally important. The development of precise manufacturing technology brings the need for more precise measuring technology. The developments in technology, especially in the field of measuring technology, have been the main reason for the increasing demands on the accuracy of the measurement. As micro and nanotechnologies have been used, it has become inevitable to develop devices and instruments that enable the measurement operations to be carried out at these accuracies.

New dimensions and research opportunities have been born in many scientific fields such as being in the electronics or molecular biology with nanotechnology. All of these disciplines are doing nanoscience studies on their own terms, and the opportunity to share all these different windows and share tools and techniques that develop independently is attractive to all sciences today. The placement of the atoms in the prescribed positions with the aid of nanotechnology is realized in this technology. Today the word “Nano” indicates a technique related to length measurements of very small objects in metrology, microtechnology, semiconductors, and nanotechnology fields. In nanometrology, the measurement size is typically specified as a nanometer. All applied methods are based on microscope technique with nano-position systems and position measurements at high accuracy. For instance, in mechanical engineering, nanotechnology and nanometrology are the necessary technologies to make a crystal perfect. The ability to precisely control the alignment of imprints and errors with respect to each other and the ability to integrate perfectly inorganic and organic nanostructures will lead to the emergence of a whole new generation of advanced composites. The improvements in technology intended to use the term *picotechnology* is a combination of picometer

and technology, parallel the term nanotechnology. Basic speckle metrology and autonomic computing resources are of course the most realistic uses of picotechnology. The ability to examine and manipulate resources at this level is quite useful. Of course, it is not difficult to imagine the tangible advantages of this type of technology.

2. Standardization in metrology

Standards are considered as measurement references. The basic standards about metrology are the basis of the traceability which is defined as a measurement whereby the result can be related to a reference through an unbroken chain of calibrations. Using internationally standardized systems of units, Vocabulary of Metrology (VIM), Guide to the International Uncertainty Measurements (GUM), or Internationally Standardized Measurement Management Systems [3] helps to improve the reliability of the results.

2.1. Unit of measurement

The most important condition of each measuring process and the manufacturing technique is the presence of units which are exactly defined according to the required quantities, and these units must be determined in accordance with internationally established rules. M*easurement* is a process that uses numbers to describe a physical quantity done to be able to compare them to each other. The results can be explained by a "*unit* of *measurement*," which is a definite magnitude of a quantity. The *SI,* The International System of *Units,* is the modern form of the metric system, and the most widely used system of measurement is made up of 7 base *units* that define the 22 derived *units* with special names and symbols. Base units provide the reference used to define all the measurement units of the system, while the derived units are products of base units and are used as measures of derived quantities. Derived units are the units obtained by algebraic operations from basic and auxiliary units. Certain derived units have special names and symbols like acceleration, meter per second squared, m s^{-2}.

2.2. Uncertainty of measurement

The uncertainty of a measurement is a predicament that characterizes the range of values, including the true value of the measure. *Measurement uncertainty* is an important topic for all measurement fields. All measurements have error. The error of a measurement is unknowable because one cannot know the error without knowing the true value of the quantity being measured. The *Evaluation of Measurement Data: Guide to the Expression of Uncertainty in Measurement* (GUM) provides general rules for evaluating and expressing uncertainty in measurement. The uncertainty of measurement generally includes many components. Some of these components can be estimated on the basis of the statistical distribution of series measurement results and can be characterized by empirical standard deviations. The estimates of the other components are based solely on the main information or experiences. The uncertainty of measurements should be evaluated and reported according to the related international standards.

2.3. Calibration

The purpose of calibration is to determine and document how much of the equipment is in error with the actual value. The correct value is obtained by considering the amount of error in the result. Calibration is the process of determining the relationship between the value read in a gauge and the gauge size. Calibration and control of measuring, inspection, and control equipments ensure the appropriateness of measurements made during manufacturing. The continuity of this safety is ensured by the regular and identifiable calibration of the equipment in question. Calibration is performed by comparison with a measurement of normality known to the measurement magnitude. To sum up, calibration is explained in the related standard: under specified conditions, the series of operations in which the relationship between the values indicated by a measuring instrument or device and the values indicated by a material measurement or reference material is established [3]. In order to supply traceability in measurements, calibration hierarchy in **Figure 1** should be followed up carefully.

3. Data evaluation

Metrology and inspection together serve as the control function of the quality of conformance. Inspection helps to evaluate the degree of conformance or nonconformance to specifications, provides for reporting of deficiencies early in the production process, and helps to assure that desired quality requirements have been met. The field of knowledge concerned with measurement. Metrology includes all aspects of both theoretical and practical with reference to measurements, whatever their level of accuracy, and in whatever fields of science or technology they occur. Since quality performance decisions are based on inspection and measurement, undesirable consequences may result if these tasks are not performed properly. Not only incorrect measurements lead to wrong decisions, which can have serious consequences, but also improper data evaluations can cause undesirable consequences. Since Statistical Process Control is the utilization of statisti-

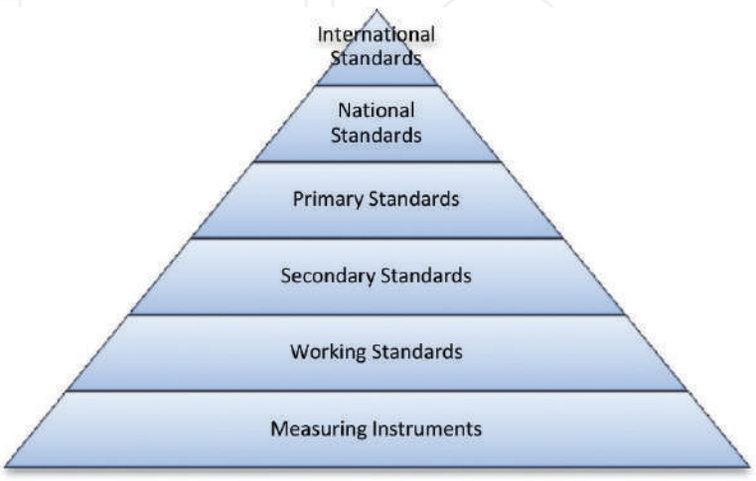

Figure 1. Hierarchy of calibration/traceability pyramid.

cal tools and methods to acquisite and to analyze data in order to monitor process capabilities, it is widely used in data evaluation. Quality control charts and the other statistical tools are used to analyze processes enabling appropriate actions to achieve improved or stabilized processes. They help to ensure that the process operates efficiently and allow organizations to understand variation in their processes, differentiating common causes from special or assignable causes of variation.

4. Conclusions

Metrology is a crucial science including its standards, systems of units, instruments, calibration procedures, uncertainties, inspection, and quality control topics in many industries such as automotive, aerospace, mechanical engineering, surface engineering, etc. and in many sciences like natural and applied sciences in different sizes like micro and nanometrology serving for sustainable improvements. Like being in today, there will always be valuable researches in the field of metrology, with the help of technological developments to support the scientific researches in the future. Care taken in the reliability of measurements and their traceability will always be crucial. Metrology is such useful for humanity if it is conducted according to its rules and international standards.

Acknowledgements

I would like to thank the authors for their contributions and the publisher that provided this opportunity.

Author details

Anil Akdogan

Address all correspondence to: nomak@yildiz.edu.tr

Mechanical Engineering Department, Yildiz Technical University, İstanbul, Turkey

References

[1] International Vocabulary of Metrology: Basic and General Concepts and Associated Terms. 3rd ed. VIM; 2012. JCGM 200:2012

[2] Uncertainty of measurement: Part 3: Guide to the expression of uncertainty in measurement. GUM; 1995. ISO/IEC Guide 98-3:2008

[3] Measurement management systems: Requirements for measurement processes and measuring equipment. 2003. ISO 10012:2003

IntechOpen

Chapter 2

Methods for Evaluation of Measurement Uncertainty

Jailton Carreteiro Damasceno and Paulo R.G. Couto

Additional information is available at the end of the chapter

http://dx.doi.org/10.5772/intechopen.74873

Abstract

This chapter presents and explains the most used methodologies for the evaluation of measurement uncertainty in metrology with practical examples. The main topics are basic concepts and importance, existing documentation, the harmonized methodology of the Guide to the Expression of Uncertainty in Measurement, types of uncertainty, modeling of measurement systems, use of alternative methods (including the GUM supplement 1 Monte Carlo numerical method), evaluation of uncertainty for calibration curves, correlated uncertainties, uncertainties arising from the calibration of instruments, and the main proposals for the new revised GUM. The chapter also discusses the GUM as a tool for the technical management of measurement processes.

Keywords: metrology, measurement, uncertainty, GUM, Monte Carlo

1. Introduction

Measurement uncertainty is a quantitative indication of the quality of measurement results, without which they could not be compared between themselves, with specified reference values or to a standard. Uncertainty evaluation is essential to guarantee the metrological traceability of measurement results and to ensure that they are accurate and reliable. In addition, measurement uncertainty must be considered whenever a decision has to be taken based on measurement results, such as in accept/reject or pass/fail processes.

Considering the context of globalization of markets, it is necessary to adopt a universal procedure for evaluating uncertainty of measurements, in view of the need for comparability of results between nations and for mutual recognition in metrology. As an example, laboratories accredited under the ISO/IEC 17025:2017 standard [1] need to demonstrate their technical

competence and the ability to properly operate their management systems, and so they are required to evaluate the uncertainty for their measurement results.

In addition, the use of uncertainty evaluation methods as a tool for technical management of measurement processes is extremely important to reduce, for example, the large number of losses that occurs in the industry, which can be highly significant in relation to the gross domestic product (GDP) of some countries. One of the probable causes of the waste can be attributed to instruments whose accuracy is inadequate to the tolerance of a certain measurement process.

In this chapter, detailed steps for uncertainty evaluation are given.

2. Main references for uncertainty evaluation

In order to harmonize the uncertainty evaluation process for every laboratory, the *Bureau International des Poids et Mesures* (BIPM) published in 1980 the Recommendation INC-1 [2] on how to express uncertainty in measurement. This document was further developed and originated the "Guide to the Expression of Uncertainty in Measurement"—GUM in 1993, which was revised in 1995 and lastly in 2008. This document provides complete guidance and references on how to treat common situations on metrology and how to deal with uncertainties in metrology. Currently, it is published by International Organization for Standardization (ISO) as the ISO/IEC Guide 98-3 "Uncertainty of measurement—Part 3: Guide to the expression of uncertainty in measurement" (GUM), and by the Joint Committee for Guides in Metrology (JCGM) as the JCGM 100:2008 guide [3]. The JCGM was established by BIPM to maintain and further develop the GUM. They are in fact currently producing a series of documents and supplements to accompany the GUM, four of which are already published [4–7].

Evaluation of uncertainty, as presented by the JCGM 100:2008, is based on the law of propagation of uncertainties (LPU). This methodology has been successfully applied for several years worldwide for a range of different measurement systems and is currently the most used procedure for uncertainty evaluation in metrology. However, since its twentieth anniversary in 2013, JCGM decided to revise it again [8–10]. In this new revision, uncertainty terms and concepts [11] will be aligned with the current International Vocabulary of Metrology (VIM) [12] and with the new GUM supplements [5, 6]. Aspects such as a new Bayesian approach, the redefinition of coverage intervals and the elimination of the Welch-Satterthwaite formula to evaluate the effective degrees of freedom will be covered [9]. In late 2014, a first draft of the newly revised version of the GUM was circulated among National Metrology Institutes. Remarkable changes were made that could affect the way laboratories deal with the measurement uncertainty results. This revision is still being discussed, and some information about it has also been released elsewhere [10].

In the field of analytical chemistry, there is also another document worth mentioning that is the "Quantifying Uncertainty in Analytical Measurement" guide [13], produced by a joint

EURACHEM/CITAC Measurement Uncertainty Working Group. This document was first published in 1995 and further revised in 2000 [14]. This last edition had a widespread implementation and is among the most highly cited publications in chemical metrology area [14]. Recently, a new revised edition was published in 2012 with improved content and added information on developments in uncertainty evaluation [14]. This document basically presents the uncertainty evaluation process following the suggestions of the GUM, but also contains several examples in the analytical chemistry area.

3. Using the GUM approach on uncertainty evaluation

The following main steps summarize the methodology presented by the GUM.

3.1. Definition of the measurand and of input quantities

It must be clear to the analyst which quantity will be the final object of the measurement in question. This quantity is known as the measurand. In addition, it is important to identify all the variables that directly or indirectly influence the measurand. These variables are known as the input quantities. As an example, Eq. (1) shows a measurand y as a function of three different input quantities: x_1, x_2, and x_3.

$$y = f(x_1, x_2, x_3) \tag{1}$$

3.2. Modeling the measurement process

In this step, the measurement procedure should be modeled in order to have a functional relationship expressing the measurand as a result of all the input quantities. The measurand y in Eq. (1) could be modeled, for example, as in Eq. (2)

$$y = \frac{x_1 x_2}{x_3^2} \tag{2}$$

The modeling step is critical for the uncertainty evaluation process as it defines how the input quantities impact the measurand. The better the model is defined, the better its representation of reality will be, including all the sources that impact the measurand on the uncertainty evaluation. The modeling process can be easily visualized by using a cause-effect diagram (**Figure 1**).

Example: To illustrate these steps, let us consider a measurement model for a torque test. Torque is a quantity that represents the tendency of a force to rotate an object about an axis. It can be mathematically expressed as the product of a force and the lever-arm distance. In metrology, a practical way to measure it is by loading a known mass to the end of a horizontal arm while keeping the other end fixed (**Figure 2**).

Note: This example is also presented, with a few adaptations, in other publications by the same authors [15].

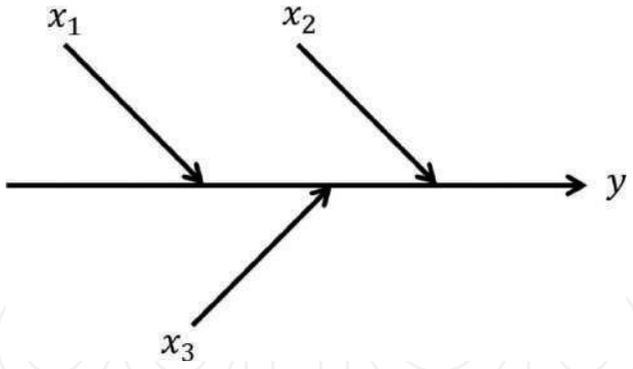

Figure 1. A cause-effect diagram representing the model from Eq. (2).

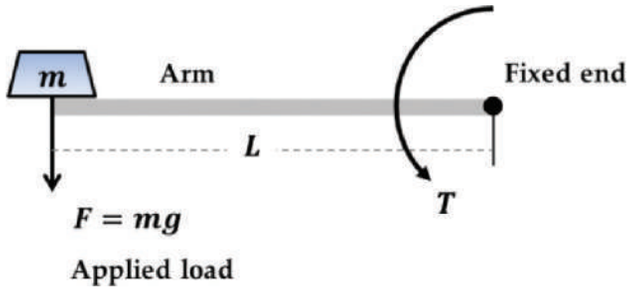

Figure 2. A conceptual illustration of the experimental setup for a measurement of torque (T), where F is the applied force, m is the mass of the load, g is the local gravity acceleration, and L is the length of the arm.

A simple model that describes this experiment can be expressed as follows:

$$T = mgL \tag{3}$$

where T is the torque (N.m), m is the mass of the applied load (kg), g is the local gravity acceleration (m/s^2), and L is the total length of the arm (m). Thus, m, g, and L are the input quantities for this model. This example will be further discussed in the subsections ahead.

3.3. Evaluating the uncertainties of the input quantities

This step is also of great importance. Here, uncertainties for all the input quantities are individually evaluated. The GUM classifies uncertainty sources as being of two main types: Type A, which usually originates from some statistical analysis, such as the standard deviation obtained in a repeatability study; and Type B, which is determined from any other source of information, such as a calibration certificate or deduced from personal experience.

Type A uncertainties from repeatability studies are evaluated by the GUM as the standard deviation of the mean obtained from the repeated measurements. For example, if a set of n indications x_i about a quantity x are available, the uncertainty u_x due to repeatability of the measurements can be expressed by $s(\overline{x})$ as follows in Eq. (4):

$$u_x = s(\overline{x}) = \frac{s(x_i)}{\sqrt{n}} \tag{4}$$

where $\overline{x}$ is the mean value of the repeated measurements, $s(x_i)$ is its standard deviation, and $s(\overline{x})$ is the standard deviation of the mean. As such, the statistical distribution associated with this input source is considered to be normal or Gaussian.

Note: This evaluation is not consistent with the GUM supplement 1 [5], where repeated indications are treated as Student's *t*-distributions to account for the lack of degrees of freedom or a low number of indications. In this way, the new proposal for the draft GUM is to consider repeated indications as *t*-distributions, just like in supplement 1. Therefore, its uncertainty would be evaluated as in Eq. (5). This equation takes the degrees of freedom for the indications $(n-1)$ into account, raising the uncertainty for a low number of indications. This correction would then be in accordance with the approach suggested by the other GUM supplements for this type of uncertainty

$$u_x = \left(\frac{n-1}{n-3}\right)^{1/2} \frac{s(x_i)}{\sqrt{n}} \tag{5}$$

It is important to note that the evaluation of uncertainties of Type B input sources must be based on careful analysis of observations or in an accurate scientific judgment, using all available information about the measurement procedure. This uncertainty type is generally used when repeated experiments would not be possible, not available, or would be too costly or time-consuming. In this case, the GUM also suggests the use of two more types of statistical distributions: the uniform and the triangular distributions.

The uniform distribution should be used when only a range of values are available, that is, an interval with the minimum and maximum values, and no detailed information about the probability of values within this interval is available. The standard uncertainty associated with such an interval is given by Eq. (6):

$$u_x = \frac{b-a}{\sqrt{12}} \tag{6}$$

where b is the maximum and a is the minimum values for the range. For example, if the only information about the room temperature of a laboratory is known to be $(20 \pm 2)^{\circ}\mathrm{C}$, then $b - a = 22 - 18 = 4^{\circ}\mathrm{C}$ and the standard uncertainty associated with the room temperature would be evaluated as $u_\theta = 4/\sqrt{12}^{\circ}\mathrm{C} = 1.15^{\circ}\mathrm{C}$.

The triangular distribution can be used when there is a strong evidence that the most probable value lies in the middle of a given interval, but still without knowing exactly how this probability behave within the interval. In chemistry, for example, the uncertainty associated with the volume of a measuring flask could be evaluated by a triangular distribution. The standard uncertainty for a triangular distribution is given by Eq. (7):

$$u_x = \frac{a}{\sqrt{6}} \tag{7}$$

where a is the semi-interval for the total range of the triangular distribution.

Another common Type B source of uncertainty is due to calibration certificates, related to a standard or to a calibrated instrument. In this case, the standard uncertainty to be used is normally obtained by dividing the expanded uncertainty U by the coverage factor k, both provided by the calibration certificate (Eq. (8))

$$u_x = \frac{U}{k} \tag{8}$$

Several good examples on how to treat some of the most common uncertainty sources can be found on the GUM [3], the EURACHEM/CITAC guide [13], and elsewhere [16].

Example: Returning to the example of torque measurement and considering the model defined in Eq. (3), the following sources of uncertainty are considered:

Mass (*m*). The mass m was repeatedly measured 10 times in a calibrated balance. The average mass was 35.7653 kg, with a standard deviation of 0.3 g. This source of uncertainty is purely statistical and is classified as being of Type A according to the GUM. The standard uncertainty (u_{m_R}) that applies in this case is obtained by Eq. (4), that is, $u_{m_R} = 0.3\ \text{g}/\sqrt{10} = 9.49 \times 10^{-5}$ kg.

In addition, the balance used for the measurement has a certificate stating an expanded uncertainty for this range of mass of U_m = 0.1 g, with a coverage factor k = 2 and a coverage probability of 95%. The uncertainty of the mass due to the calibration of the balance constitutes another source of uncertainty involving the same input quantity (mass). In this case, the standard uncertainty (u_{m_C}) is calculated by using Eq. (8), that is, $u_{m_C} = U_m/k = 0.1\ \text{g}/2 = 0.00005$ kg.

Local gravity acceleration (*g*). The value for the local gravity acceleration is stated in a certificate of measurement as 9.80665 m/s^2, as well as its expanded uncertainty of U_g = 0.00002 m/s^2, for k = 2 and p = 95%. Again, Eq. (8) is used to calculate the standard uncertainty (u_g), that is, $u_g = U_g/k = \left(0.00002\ \text{m/s}^2\right)/2 = 0.00001\ \text{m/s}^2$.

Length of the arm (*L*). Let us suppose that in this hypothetical case, the arm used in the experiment has no certificate of calibration, indicating its length value and uncertainty, and that the only measuring method available for the arm's length is by the use of a ruler with a minimum division of 1 mm. The use of the ruler leads then to a measurement value of 2000.0 mm for the length of the arm. However, in this situation, very poor information about the measurement uncertainty of the arm's length is available. As the minimum division of the ruler is 1 mm, one can assume that the reading can be done with a maximum accuracy of up to 0.5 mm, which can be thought as an interval of ±0.5 mm as limits for the measurement. As no information of probabilities within this interval is available, the assumption of a uniform distribution is the best option, on which there is equal probability for the values within the whole interval. Thus, Eq. (6) is used to determine the standard uncertainty (u_L), that is, $u_L = (2000.5 - 1999.5)\ \text{mm}/\sqrt{12} = 0.000289$ m.

In practice, one can imagine several more sources of uncertainty for this experiment, like, for example, the thermal dilatation of the arm as the room temperature changes. However, the objective here is not to exhaust all the possibilities, but instead to provide basic notions of how to implement the methodology of the GUM on a simple model.

3.4. Propagation of uncertainties

3.4.1. The law of propagation of uncertainties

The GUM uncertainty approach is based on the law of propagation of uncertainties (LPU). This methodology encompasses a set of approximations to simplify the calculations and is valid for a range of simplistic models.

According to the LPU, the propagation of uncertainties is accomplished by expanding the measurand model in a Taylor series and simplifying the expression by considering only the first-order terms. This approximation is viable as uncertainties are very small numbers compared with the values of their corresponding quantities. In this way, the treatment of a model where the measurand y is expressed as a function of N variables $x_1, \ldots, x_N$ (Eq. (9)) leads to the general expression for the propagation of uncertainties shown in Eq. (10)

$$y = f(x_1, \ldots, x_N) \tag{9}$$

$$u_y^2 = \sum_{i=1}^{N} \left(\frac{\partial y}{\partial x_i}\right)^2 u_{x_i}^2 + 2\sum_{i=1}^{N-1}\sum_{j=i+1}^{N} \left(\frac{\partial y}{\partial x_i}\right)\left(\frac{\partial y}{\partial x_j}\right) COV(x_i, x_j) \tag{10}$$

where u_y is the combined standard uncertainty for the measurand y and u_{x_i} is the uncertainty for the ith input quantity. The second term of Eq. (10) is due to the correlation between the input quantities. If there is no supposed correlation between them, Eq. (10) can be further simplified as

$$u_y^2 = \sum_{i=1}^{N} \left(\frac{\partial y}{\partial x_i}\right)^2 u_{x_i}^2 \tag{11}$$

The partial derivatives of Eq. (11) are known as sensitivity coefficients and describe how the output estimate y varies with changes in the values of the input estimates $x_1, x_2, \ldots, x_N$. It also converts the units of the inputs to the unit of the measurand.

Another important observation regarding the sensitivity coefficient occurs when the mathematical model that defines the measurand does not contemplate a given quantity, known as influence quantity. In this case, the determination of the sensitivity coefficient of the measurand in relation to the input quantity must be done experimentally. For example, biodiesel is susceptible to oxidation when exposed to air, and this oxidation process affects fuel quality. The oxidation time is determined by measuring the conductivity of an oil sample when inflated with air at a given flow rate. There are a number of influence quantities that impact the oxidation time of biodiesel such as temperature, air flow, conductivity, sample mass, and so on. In this case, the sensitivity coefficients for oxidation time with respect to each of these influence quantities are determined from an interpolation function obtained with experimental data. For example, **Figure 3** presents the table and its resulting graph, which shows the model of the function that relates the oxidation time to the temperature of a biofuel sample (case study of the authors).

Temperature [°C]	Oxidation time [h]
100	17.31
100	16.60
100	17.00
110	9.14
110	9.19
110	9.27
120	4.06
120	4.01
120	3.93

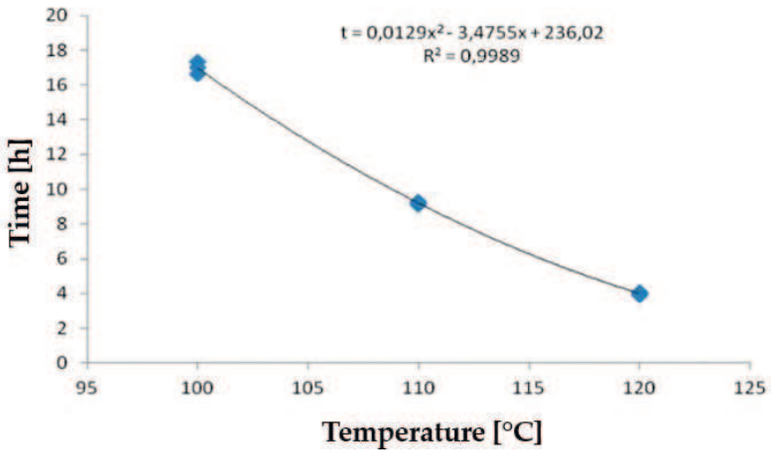

Figure 3. A table and a graph representing the variation of the oxidation time of a biofuel sample as a function of temperature.

Example: On returning to the torque measurement example, assuming that all the input quantities are independent, the combined standard uncertainty for the torque is calculated by using the LPU (Eq. (11)). The final expression is then

$$u_T = \sqrt{\left(\frac{\partial T}{\partial m}\right)^2 u_{m_R}^2 + \left(\frac{\partial T}{\partial m}\right)^2 u_{m_C}^2 + \left(\frac{\partial T}{\partial g}\right)^2 u_g^2 + \left(\frac{\partial T}{\partial L}\right)^2 u_L^2} = 0.096 \text{ N m} \tag{12}$$

It is important to note that the terms (not squared) of Eq. (12), that is, each sensitivity coefficient multiplied by its corresponding uncertainty, are known as uncertainty components. These components can be compared to each other as they are in the same units of the measurand. **Figure 4** shows the comparison between the uncertainty components for the torque measurement model.

As can be noted, the dominant uncertainty component is due to the uncertainty associated with the measurement of the arm length, which was taken as the resolution of the non-calibrated

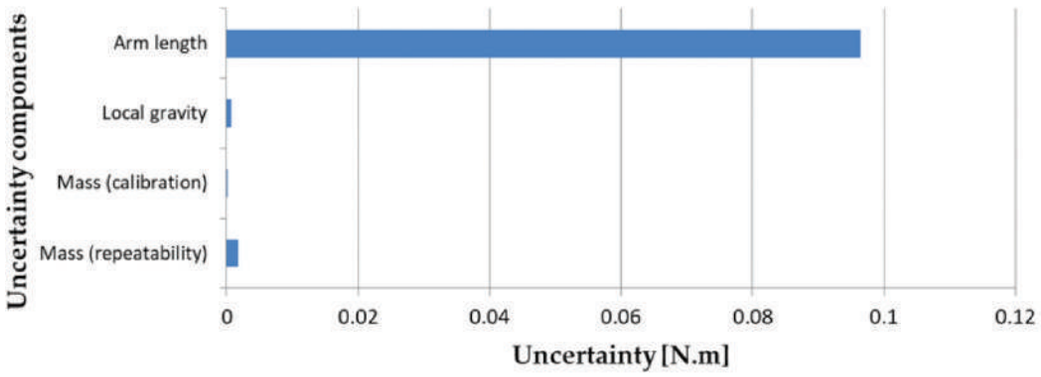

Figure 4. Uncertainty component balance for the input quantities in the torque measurement model.

ruler used in the measurement. This analysis shows to the analyst that, to reduce the final uncertainty and improve the measurement system, a calibrated ruler, with a better uncertainty, should be used. This represents the importance of the GUM as a management tool to the measurement process.

3.4.2. The Kragten method

The Kragten method is an approximation that facilitates the calculation of the combined uncertainty using finite differences in place of the derivatives [13]. This approximation is valid when the uncertainties of the inputs are relatively small compared to the respective values of the input quantities, generating discrepancies in the final result in relation to the LPU that occur in decimals that can be ignored.

Assuming a measurand y, which is calculated from the input quantities x_1, x_2 and x_3 according to the mathematical model of Eq. (2), the uncertainties u_{x_1}, u_{x_2} and u_{x_3} for the input quantities are evaluated normally, according to methodologies already explained previously. From there, the calculations of the measurand are performed individually for each input magnitude (y_{x_1}, y_{x_2} and y_{x_3}) so that each time their respective values are added with their uncertainties, as shown in Eqs. (13)–(15)

$$y_{x_1} = \frac{(x_1 + u_{x_1})x_2}{x_3^2} \tag{13}$$

$$y_{x_2} = \frac{x_1(x_2 + u_{x_2})}{x_3^2} \tag{14}$$

$$y_{x_3} = \frac{x_1 x_2}{(x_3 + u_{x_3})^2} \tag{15}$$

The value of the measurand y varies for y_{x_i} due to the addition of the uncertainty u_{x_i} to the value of its respective input quantity. Thus, the uncertainty component of each input source in the unit of the measurand y is defined by the difference $\left|y_{x_i} - y\right|$, according to Eqs. (16)–(18)

$$u_y(x_1) = \left|y_{x_1} - y\right| \tag{16}$$

$$u_y(x_2) = \left|y_{x_2} - y\right| \tag{17}$$

$$u_y(x_3) = \left|y_{x_3} - y\right| \tag{18}$$

Thus, the combined standard uncertainty of y is finally evaluated as

$$u_y = \sqrt{\sum_{i=1}^{N} u_y^2(x_i)} \tag{19}$$

or by Eq. (20), if there are correlated uncertainties

$$u_y = \sqrt{\sum_{i=1}^{N} u_y^2(x_i) + 2\sum_{i=1}^{N-1}\sum_{j=i+1}^{N} u_y(x_i)u_y(x_j)r(x_i,x_j)} \tag{20}$$

where $r(x_i, x_j)$ is the correlation coefficient between x_i and x_j.

3.5. Evaluation of the expanded uncertainty

The result provided by Eqs. (10) and (11) corresponds to an interval that contains only one standard deviation (or approx. 68.2% of the measurements for a normal distribution). In order to have a better coverage probability for the result, the GUM approach expands this interval by assuming that the measurand follows the behavior of a Student's *t*-distribution. An effective degrees of freedom v_{eff} for the *t*-distribution can be obtained by using the Welch-Satterthwaite formula (Eq. (21))

$$v_{eff} = \frac{u_y^4}{\sum_{i=1}^{N} \frac{\left(\frac{\partial y}{\partial x_i}\right)^4 u_{x_i}^4}{v_{x_i}}} \tag{21}$$

where v_{x_i} is the degrees of freedom for the *i*th input quantity.

The effective degrees of freedom is used to obtain a coverage factor k that depends also of a chosen coverage probability p, which is often 95%. The expanded uncertainty U_y is then evaluated by multiplying the combined standard uncertainty by the coverage factor k that finally expands it to a coverage interval delimited by a *t*-distribution with a coverage probability p (Eq. (22))

$$U_y = ku_y \tag{22}$$

Note: The draft for the new GUM proposal suggests that the final coverage interval cannot be reliably determined if only an expectation y and a standard deviation u_y are known, mainly if the final distribution deviates significantly from a normal or a *t*-distribution. Thus, they propose distribution-free coverage intervals in the form of $y \pm U_p$, with $U_p = k_p u_y$: (a) if no information is known about the final distribution, then a coverage interval for the measurand Y for coverage probability of at least p is determined using $k_p = 1/(1-p)^{1/2}$. If $p = 0.95$, a coverage interval of $y \pm 4.47u_y$ is evaluated. (b) If it is known that the distribution is unimodal and symmetric about y, then $k_p = 2/\left[3(1-p)^{1/2}\right]$ and the coverage interval $y \pm 2.98u_y$ would correspond to a coverage probability of at least $p = 0.95$.

Example: The effective degrees of freedom for the torque measurement example is calculated using Eq. (21). As the number of degrees of freedom for Type B uncertainties is considered infinite, only Type A uncertainties are accounted. In this case,

$$v_{eff} = \frac{u_T^4}{\frac{\left(\frac{\partial T}{\partial m_R}\right)^4 u_{m_R}^4}{v_{m_R}}} = 6.5 \times 10^7 \tag{23}$$

Using t-distribution tables, the coverage factor for this value of υ_{eff} and p = 95% is k = 1.96. Therefore, the expanded uncertainty is calculated as $U = ku_T = 1.96 \times 0.096 = 0.2$ N m, and the measurement result is expressed as 668.0 ± 0.2 N m. The GUM recommends that the final uncertainty should be expressed with one or at most two significant digits.

4. Calibration curve and correlated uncertainties

One of the most valuable tools for the metrologist is the calibration curve. It is widely used in measurement systems on which one cannot directly obtain the property value to be measured of an object. Instead, a response from the system is measured. In this way, a calibration curve is used to correlate the response from the system with well-known property values, usually calibration standards (see **Figure 5**).

With a calibration curve in hands, the property value for a new unknown sample can be directly determined by using the equation for the fitted curve, which is usually adjusted by a linear regression. However, the calibration curve contains errors due to the lack of fit for the experimental data, causing an uncertainty source to arise. Thus, when evaluating the uncertainty for a predicted property value of x_o corresponding to a new observation y_o (for a new unknown sample, for example), the LPU with correlation terms is applied on the linear regression model in the form of Eq. (24). Eq. (25) represents the model for a predicted value y_o corresponding to a new observed value x_o, in the case of the inverse process

$$x_0 = \frac{y_o - a}{b} \tag{24}$$

$$y_o = a + bx_0 \tag{25}$$

where a and b are, respectively, the intercept and the slope parameters of the linear regression.

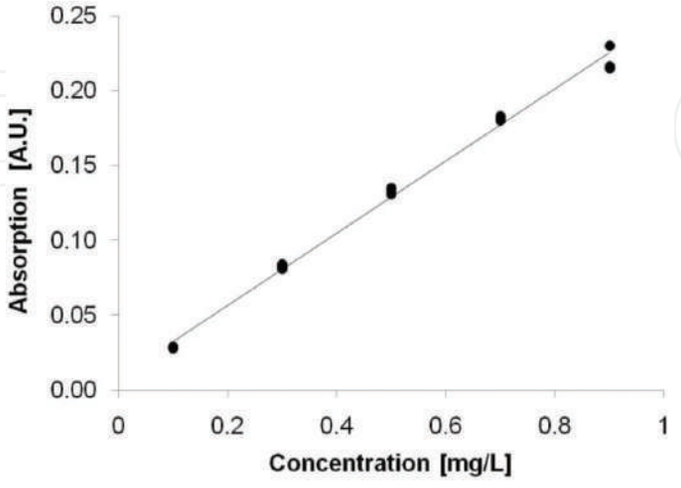

Figure 5. An example of a linear calibration curve for atomic absorption spectroscopy: the absorption signals (instrument responses) are plotted against the concentrations for a specific analyte.

The application of the LPU with the correlation term to Eqs. (24) and (25) leads to Eqs. (26) and (27), respectively, for both cases:

$$u_{x_o} = \sqrt{\left(\frac{\partial x_o}{\partial y_o}\right)^2 u_{y_o}^2 + \left(\frac{\partial x_o}{\partial a}\right)^2 u_a^2 + \left(\frac{\partial x_o}{\partial b}\right)^2 u_b^2 + 2\left(\frac{\partial x_o}{\partial a}\right)\left(\frac{\partial x_o}{\partial b}\right) u_a u_b r_{a,b}} \tag{26}$$

$$u_{y_o} = \sqrt{\left(\frac{\partial y_o}{\partial x_o}\right)^2 u_{x_o}^2 + \left(\frac{\partial y_o}{\partial a}\right)^2 u_a^2 + \left(\frac{\partial y_o}{\partial b}\right)^2 u_b^2 + 2\left(\frac{\partial y_o}{\partial a}\right)\left(\frac{\partial y_o}{\partial b}\right) u_a u_b r_{a,b}} \tag{27}$$

For Eq. (26), u_{x_o} is the combined uncertainty for the predicted value x_o and u_{y_o} is the uncertainty for the new observed response y_o. For Eq. (27), u_{y_o} is the combined uncertainty for the predicted value y_o and u_{x_o} is the uncertainty for the new observed response x_o. In both cases, u_a and u_b are, respectively, the uncertainties for the intercept and the slope, and $r_{a,b}$ is the correlation coefficient between a and b. These last equations can also be found in the ISO/TS 28037 [17], concerning the use of straight-line calibration functions.

The uncertainties for a and b can be obtained by Eqs. (28) and (29), respectively, while the correlation coefficient $r_{a,b}$ is given by Eq. (30)

$$u_a = S_e \sqrt{\frac{\sum x_i^2}{n\sum x_i^2 - \left(\sum x_i\right)^2}} \tag{28}$$

$$u_b = S_e \sqrt{\frac{n}{n\sum x_i^2 - \left(\sum x_i\right)^2}} \tag{29}$$

$$r_{a,b} = -\frac{\sum x_i}{\sqrt{n\sum x_i^2}} \tag{30}$$

where n is the number of points used to construct the curve, x_i are the values for the independent variable of the linear equation for each y_i, and S_e^2 is the residual variance of the fitted curve, obtained by Eq. (31)

$$S_e^2 = \frac{\sum \left(y_i - \widehat{y}_i\right)^2}{n-2} \tag{31}$$

where $\widehat{y}_i$ are the interpolated values in the fitted curve for each x_i, that is, $\widehat{y}_i = a + bx_i$.

Example: This time, let us consider that the calibration certificate of a thermometer presents the results shown in **Table 1**.

For the data shown in **Table 1**, the calibration curve of the thermometer is expressed by $\widehat{y}_o = 1.1484 + 0.9578x_o$. For a temperature value indicated by the thermometer of x_o = 22°C, applying the equation of the calibration curve yields a reference value of $\widehat{y}_o$ = 22.22°C.

Indication (x_i) (°C)	Reference value (y_i) (°C)
20	20.3
21	21.3
22	22.2
23	23.1
24	24.2
25	25.1
27	27.0

Table 1. Values of the calibration certificate of a thermometer.

Using Eqs. (28)–(31), it is possible to calculate the values of **Table 2** that shows the statistical data for the thermometer calibration curve.

Considering that there is no uncertainty for the observed point x_o = 22°C, that is, u_{x_o} = 0, the uncertainty of y_o arising from the interpolation process of the point x_o = 22°C can then be calculated by applying Eq. (27) and the data from **Table 2**, resulting in the following: $u_{y_o} = \sqrt{1^2 \cdot 0.1943^2 + 22^2 \cdot 0.0084^2 + 2 \cdot 1 \cdot 22 \cdot 0.1943 \cdot 0.0084 \cdot (-0.995)} = 0.021°\text{C}$.

Another frequently used expression for the standard uncertainty of the predicted value u_{x_o} is given by Eq. (32) [13, 18]:

$$u_{x_o} = \frac{S_e}{b}\sqrt{\frac{1}{m} + \frac{1}{n} + \frac{\left(\overline{y}_o - \overline{y}\right)^2}{b^2 \sum \left(x_i - \overline{x}\right)^2}} \tag{32}$$

where S_e is the residual standard deviation of the fitted line, m is the number of observations of y_o, n is the number of points composing the calibration curve, and $\overline{y}_o$ is the average value obtained from the observations of y_o. In this expression, the uncertainty component due to the observations of y_o is evaluated by [19]

$$u_{y_o} = \frac{S_e}{\sqrt{m}} \tag{33}$$

However, Hibbert [19] suggests that if the standard deviation of the indications is known from consistent data, u_{y_o} can be better evaluated by

Data	Value	Unit
S_e^2	0.0024	°C^2
u_a	0.1943	°C
u_b	0.0084	
$r_{a,b}$	−0.995	

Table 2. Statistical data for the calibration curve of a thermometer.

$$u_{y_o} = \frac{S_{y_o}}{\sqrt{m}} \tag{34}$$

where S_{y_o} is the standard deviation of the observations of y_o, and Eq. (32) is then expressed as Eq. (35) [18, 19]:

$$u_{x_o} = \frac{1}{b}\sqrt{\frac{S_{y_o}^2}{m} + \frac{S_e^2}{n} + \frac{S_e^2\left(\overline{y}_o - \overline{y}\right)^2}{b^2\sum\left(x_i - \overline{x}\right)^2}} \tag{35}$$

5. Assessment of uncertainty in instrument calibration

The methodology presented in the GUM can also be used to evaluate the uncertainty in the calibration of a measuring instrument. Following the steps of the GUM, the measurand for the model used in the calibration must be defined by the quantity that evaluates the systematic error of an instrument over its entire measurement range. Thus, Eq. (36) can be generally used for the evaluation of uncertainty in a calibration process:

$$e = V_{ind} - V_{ref} \tag{36}$$

where e is the systematic error of the instrument for a fixed range, V_{ind} is the value indicated by the instrument, and V_{ref} is the reference value corresponding to the indicated value.

From Eq. (36), a basic cause-and-effect diagram can be assembled for the calibration uncertainty assessment of an instrument, as shown in **Figure 6**.

The sources of uncertainty in this case involve the repeatability of indicated values, the resolution of the instrument in calibration, and the certificate of calibration of the reference values. Thus, an evaluation of the uncertainty about the systematic error should be done for each nominal value of the instrument in calibration. The combined standard uncertainties u_{ei} for each calibrated nominal value are obtained by applying the LPU, as shown in Eq. (37)

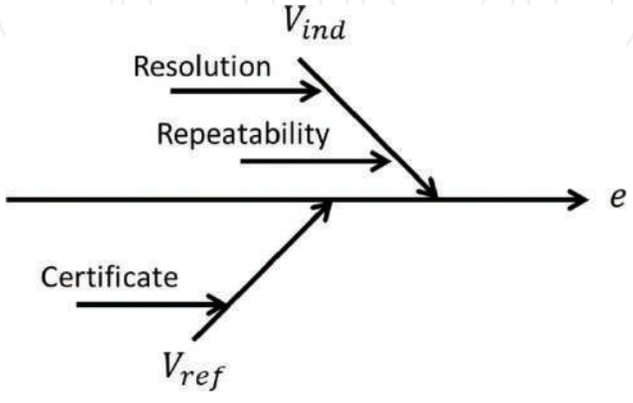

Figure 6. A general cause-and-effect diagram for the calibration of an instrument.

$$u_{e_i} = \sqrt{\left(\frac{\partial e_i}{\partial V_{ind}}\right)^2 u^2_{V_{ind_{Res}}} + \left(\frac{\partial e_i}{\partial V_{ind}}\right)^2 u^2_{V_{ind_{Rep}}} + \left(\frac{\partial e_i}{\partial V_{ref}}\right)^2 u^2_{V_{ref}}} \tag{37}$$

where $u_{V_{ind_{Res}}}$, $u_{V_{ind_{Rep}}}$, and $u_{V_{ref}}$ are, respectively, standard uncertainties due to resolution of the instrument, repeatability of indication values, and certificate of calibration of the reference. These standard uncertainties are obtained as described in Section 3.

The final calibration result can then be presented according to **Table 3**. In addition, correction values or systematic errors can also be reported.

6. Monte Carlo simulation applied to metrology

This section presents the limitations of the GUM and shows an alternative methodology based on the propagation of distributions that overcome those limitations. For further details, please refer to the authors' publication that addresses the use of the Monte Carlo methodology applied to uncertainty in measurement [15] or to the JCGM 101:2008 guide [5]. Also, in the field of analytical chemistry, the latest version of EURACHEM/CITAC guide (2012) was updated with procedures to use Monte Carlo simulations [13].

6.1. Limitations of the GUM approach

As mentioned earlier, the approach to evaluate measurement uncertainties using the LPU as presented by the GUM is based on some approximations that are not valid for every measurement model [5, 20–22]. These approximations comprise (1) the linearization of the measurement model made by the truncation of the Taylor series, (2) the use of a *t*-distribution as the distribution for the measurand, and (3) the calculation of an effective degrees of freedom for the measurement model based on the Welch-Satterthwaite formula, which is still an unsolved problem [23]. Moreover, the GUM approach usually presents deviated results when one or more of the input uncertainties are relatively much larger than others, or when they have the same order of magnitude than its quantity.

The limitations and approximations of the LPU are overcome when using a methodology that relies on the propagation of distributions. This methodology carries more information than the simple propagation of uncertainties and generally provides results closer to reality. It is

Range	Indicated value	Reference value	Expanded uncertainty	Coverage factor
Range 1	V_{ind1}	V_{ref1}	U_1	k_1
Range 2	V_{ind2}	V_{ref2}	U_2	k_2
…	…	…	…	…
Range N	V_{indN}	V_{refN}	U_N	k_N

Table 3. A typical format for the result of calibration of an instrument.

described in detail by the JCGM 101:2008 guide (Evaluation of measurement data—Supplement 1 to the "Guide to the expression of uncertainty in measurement"—propagation of distributions using a Monte Carlo method) [5], providing basic guidelines for using Monte Carlo numerical simulations for the propagation of distributions in metrology. This method provides reliable results for a wider range of measurement models as compared to the GUM approach and is presented as a fast and robust alternative method for cases where the GUM approach does not present good results.

6.2. Running Monte Carlo simulations

The propagation of distributions as presented by the JCGM 101:2008 involves the convolution of the probability distributions for the input sources of uncertainty through the measurement model to generate a distribution for the output (the measurand). In this process, no information is lost due to approximations, and the result is much more consistent with reality.

The main steps of this methodology are similar to those presented in the GUM. The measurand must be defined as a function of the input quantities through a model. Then, for each input, a probability density function (PDF) must be assigned. In this step, the concept of maximum entropy used in the Bayesian statistics should be used to assign a PDF that does not contain more information than that which is known by the analyst. A number of Monte Carlo trials are then chosen and the simulation can be set to run.

Results are expressed in terms of the average value for the output PDF, its standard deviation, and the end points that cover a chosen probability p.

Example: Returning once more to the torque measurement example, one can consider the following PDFs for the input sources:

Mass (m). For repeated indications, the JCGM 101:2008 suggests the use of a scaled and shifted t-distribution. Thus, the distribution should use 35.7653 kg as its average, a scale value of $s/\sqrt{n} = 0.3\ \text{g}/\sqrt{10} = 9.49 \times 10^{-5}$ kg, and $n - 1 = 9$ degrees of freedom.

For the calibration component, the supplement 1 recommends the use of a normal distribution if the number of degrees of freedom is not available. In this case, the mass value of 35.7653 kg is taken as the mean and a standard deviation of $U_m/k = 0.1\ \text{g}/2 = 0.00005$ kg should be used. However, to facilitate the calculation of the final mean value of the measurand, the mean should be shifted to zero, since both values for the mass sources will be added together.

Local gravity acceleration (g). This case is similar to the case of the balance certificate, for which we have values of expanded uncertainty and coverage factor without information on the number of effective degrees of freedom. Thus, a normal distribution with a mean of 9.80665 m/s^2 and a standard deviation of $U_g/k = (0.00002\ \text{m/s2})/2 = 0.00001$ m/s^2 are assumed.

Length of the arm (L). In this case, as poor information about the interval is available ($\pm$0.5 mm), an uniform distribution is assumed with a minimum value of 1999.5 mm and a maximum value of 2000.5 mm.

Uncertainty source	Type	PDF	PDF parameters
Mass (repeatability)	A	*t*-distribution	Mean: 35.7653 kg; scale: 9.49 x 10^{-5} kg; degrees of freedom: 9
Mass (certificate)	B	Normal	Mean: 0 kg; standard deviation: 0.00005 kg
Local gravity	B	Normal	Mean: 9.80665 m/s^2; standard deviation: 0.00001 m/s^2
Arm length	B	Uniform	Minimum: 1999.5 mm; maximum: 2000.5 mm

Table 4. A summary of sources of uncertainty and their associated distributions for the measurement of torque.

Table 4 resumes the input information for the simulation, which was executed for $M = 200,000$ trials, generating the output distribution shown in **Figure 7**.

Table 5 summarizes the statistical data of the output distribution, including the upper and lower limits of a probabilistically symmetric range for a 95% coverage probability.

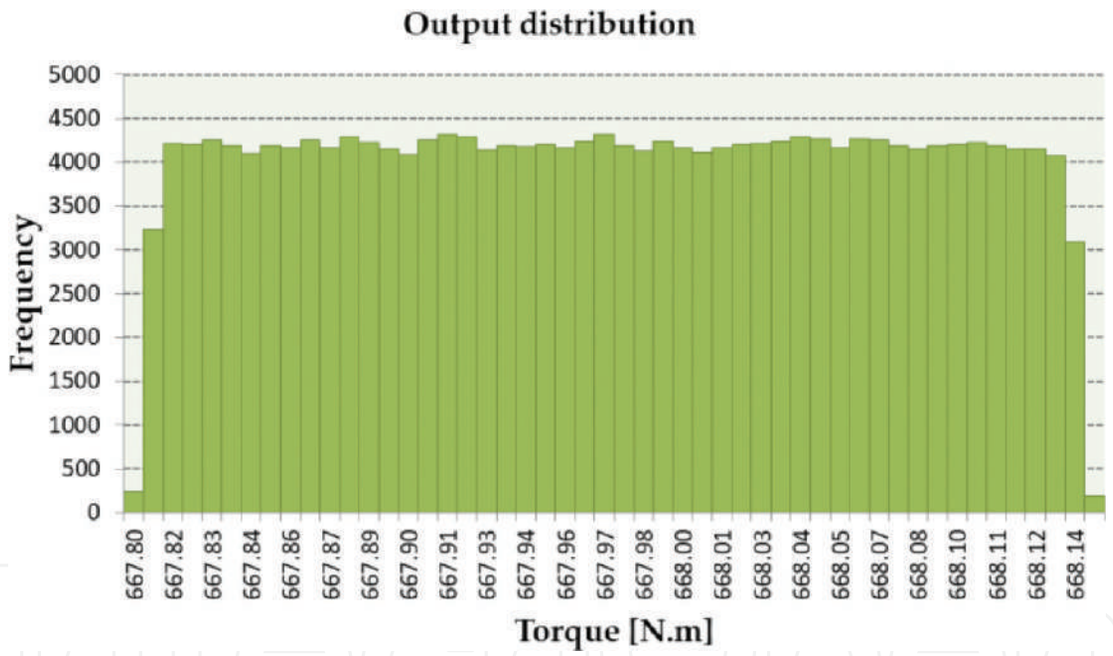

Figure 7. Output distribution resulting from the Monte Carlo simulation for the evaluation of uncertainty of measurement of torque.

Statistical data	Value (N m)
Mean	667.970
Standard deviation	0.096
Lower limit for p = 95%	667.812
Upper limit for p = 95%	668.129

Table 5. A summary of the statistical data for the output distribution for the measurement of torque.

7. Conclusions

Measurement uncertainty and metrological traceability are interdependent concepts. The evaluation of uncertainties of measurement results is essential to ensure that they are reliable and comparable. Moreover, the process that involves the modeling of measurement systems and evaluation of their uncertainties is of great importance for the metrologist as it constitutes a tool for the management of the measurement laboratory, since it can indicate exactly where to invest to get better, more qualified results.

The GUM and the application of the LPU continue to be the most used and widespread methodology for bottom-up uncertainty evaluation in metrology. It is adopted worldwide and provides a strong base for comparability of measurement results between laboratories. On the other hand, a new version for the GUM is currently under revision. This version should be aligned with its supplements in a more harmonized way, incorporating concepts from Bayesian statistics and resolving some inconsistencies. As a consequence, if the mentioned distribution-free coverage intervals are maintained, results for the expanded uncertainty will be greatly overestimated compared to the current version of the GUM.

In this way, the best alternative for a more realistic and lean uncertainty assessment would be through a numerical simulation using the Monte Carlo method, which should lead to a smaller and more reliable uncertainty result.

Author details

Jailton Carreteiro Damasceno* and Paulo R.G. Couto

*Address all correspondence to: jcdamasceno@inmetro.gov.br

National Institute of Metrology, Quality and Technology (Inmetro), Rio de Janeiro, Brazil

References

[1] ISO/IEC 17025. 2005. General Requirements for the Competence of Testing and Calibration Laboratories. ISO: Geneva

[2] Kaarls R. BIPM Proc.-Verb. Com. Int. Poids et Mesures 49:A1–12 (in French), Giacomo P (1981). Metrologia. 1981;**17**:73-74 (in English)

[3] JCGM 100:2008. Evaluation of measurement data—Guide to the expression of uncertainty in measurement. Joint Committee for Guides in Metrology, 2008

[4] JCGM 104:2009. Evaluation of measurement data—An introduction to the "Guide to the expression of uncertainty in measurement" and related documents. Joint Committee for Guides in Metrology. 2009

[5] JCGM 101:2008. Evaluation of measurement data—Supplement 1 to the "Guide to the expression of uncertainty in measurement"—Propagation of distributions using a Monte Carlo method. Joint Committee for Guides in Metrology. 2008

[6] JCGM 102:2011. Evaluation of measurement data—Supplement 2 to the "Guide to the expression of uncertainty in measurement"—Extension to any number of output quantities. Joint Committee for Guides in Metrology. 2011

[7] JCGM 106:2012. Evaluation of measurement data—The role of measurement uncertainty in conformity assessment. Joint Committee for Guides in Metrology. 2012

[8] Bich W, Cox MG, Dybkaer R, Elster C, Estler WT, Hibbert B, Imai H, Kool W, Michotte C, Nielsen L, Pendrill L, Sidney S, van der Veen AMH, Woger W. Revision of the 'guide to the expression of uncertainty in measurement'. Metrologia. 2012;**49**:702-705

[9] Bich W. Revision of the 'guide to the expression of uncertainty in measurement'—Why and how. Metrologia. 2014;**51**:S155-S158

[10] Bich W, Cox M, Michotte C. Towards a new GUM—An update. Metrologia. 2016;**53**:S149-S159

[11] Ehrlich C. Terminological aspects of the guide to the expression of uncertainty in measurement (GUM). Metrologia. 2014;**51**:S145-S154

[12] JCGM 200:2012. International vocabulary of metrology—basic and general concepts and associated terms (VIM). Joint Committee for Guides in Metrology. 2012

[13] EURACHEM/CITAC Guide CG4. Quantifying uncertainty in analytical measurement. EURACHEM/CITAC. 2012

[14] Ellison SLR. Implementing measurement uncertainty for analytical chemistry: The Eurachem guide for measurement uncertainty. Metrologia. 2014;**51**:S199-S205

[15] Couto PRG, Damasceno JC, Oliveira SP. Chapter 2—Monte Carlo simulations applied to uncertainty in measurement. In: Chan V, editor. InTech: Theory and Applications of Monte Carlo Simulations; 2013

[16] Meyer VR. Measurement uncertainty. Journal of Chromatography. A. 2007;**1158**:15-24

[17] ISO/TS 28037. Determination and Use of Straight-line Calibration Functions. Geneva: ISO; 2010

[18] Massart DL, Vandeginste BGM, Buydens LMC, Jong S, Lewi PJ, Smeyers-Verbeke J. Data Handling in Science and Technology. v. 20. Handbook of Chemometrics and Qualimetrics: Part A. Amsterdam: Elsevier; 1997

[19] Hibbert DB. The uncertainty of a result from a linear calibration. Analyst. 2006;**131**:1273-1278

[20] Harris PM, Cox MG. On a Monte Carlo method for measurement uncertainty evaluation and its implementation. Metrologia. 2014;**51**:S176-S182

[21] Possolo A. Statistical models and computation to evaluate measurement uncertainty. Metrologia. 2014;**51**:S228-S236

[22] Gonzalez AG, Herrador MA, Asuero AG. Uncertainty evaluation from Monte-Carlo simulations by using Crystal-Ball software. Accreditation and Quality Assurance. 2005; **10**:149-154

[23] Lepek A. A computer program for a general case evaluation of the expanded uncertainty. Accreditation and Quality Assurance. 2003;**8**:296-299

IntechOpen

Chapter 3

Variational Calibration

Michael Surdu

Additional information is available at the end of the chapter

http://dx.doi.org/10.5772/intechopen.74220

Abstract

The approach to the improving the accuracy of the impedance parameter measurements is described. This approach is based on the well-known variations of the influence of the disturbing factors on the results of measurement. Using these variations, measurement circuit provides the additional number of measurements, equal to the number of the disturbing factors. System of equations describes these results of measurements. The solution of this system eliminates the influence of the appropriate uncertainty sources on the results of measurement and gets the true result of the measured value. In addition, the solution of this system also gets the values of the uncertainty components in every measurement and possibility to monitor the properties of the measurement circuit. Examples of the realization of this method for improving the accuracy of the impedance parameter measurements in different bridges are given.

Keywords: impedance, variation calibration, uncertainty, measurement, algorithm, comparison, quadrature, standard, digital synthesis, frequency range, transfer's function

1. Introduction

History of the electricity science is the history of the development, in sufficient part, of the new methods of measurements. These methods are described perfectly well, for example, in [1]. Widely used replacing and substitution methods entered in all handbooks [2]. Bridge methods are described in many monographs [3, 4]. Monographs [5, 6] describe different methods of bridges' accurate balance. Many methods of uncertainty correction are described in [7, 8]. All these methods have their widely discussed advantages and disadvantages. There exists no method that could decide all problems, which appears in measuring practice. This chapter describes the method of the variational calibration [9] in the impedance measurements. This method is based on the *sequential* variation of the influence of the disturbing factors on the

results of measurement. System of equations describes these results. Solution of this system eliminates influences of the disturbing factors and gets the accurate results of measurement. This method significantly simplifies the accurate devices, reducing their weight, dimension and cost, but increases the time of measurement.

2. The variational calibration

2.1. Theoretical basis of the variational calibration

Every measuring circuit (MC) has the input value, which has to be measured and generates measured output value. In an ideal case, the results of measurement depend on the input value and the transfer function ***k*** of the MC only.

Formula (1) describes the result of measurement of ideal MC:

$$Z_x = kZ_0 \tag{1}$$

Formula (2) describes the standard uncertainty δ_{id} of such measurement:

$$\delta_{id} = \sqrt{\delta_0^2 + \delta_s^2} \tag{2}$$

Here δ_0 and δ_s are the uncertainties, of the standard Z_0 and the uncertainty, caused by the sensitivity of the MC.

In the real MC, the results of measurement Z_{x0} also depend on the complex of the disturbing factors $z_1 \ldots z_i \ldots z_j$ as well (for simplicity of the description, these factors on the **Figure 1** are shown being out of MC). These factors create proper complex of the uncertainties of measurements $\delta_1 \ldots \delta_i \ldots \delta_j$ and shift the appropriate result Z_{x0} of measurement from its ideal value Z_x.

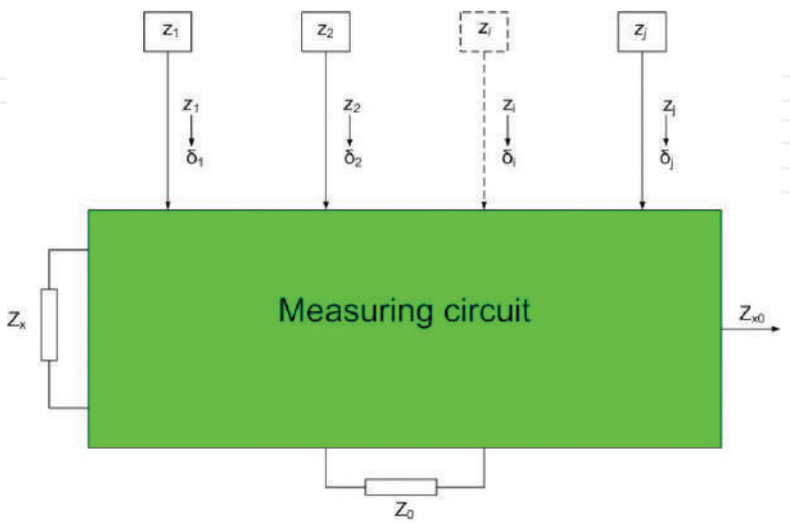

Figure 1. Real measuring circuit.

http://dx.doi.org/10.5772/intechopen.74220

The much more complicated mathematic model (3) of the real MC now describes the results of measurement:

$$Z_{x0} = \gamma\left(Z_x; \delta_1 \ldots \delta_i \ldots \delta_j; \delta_0; \delta_s\right) \tag{3}$$

Usually the model (3) is well known from preliminary investigations of the MC.

In the simplest case, every disturbing factor $z_1..z_i..z_j$ creates appropriate uncertainty components $\delta_1 \ldots \delta_i \ldots \delta_j$. In more complicated cases, some disturbing factors $z_1 \ldots z_i$ can influence some complex $Z_i \ldots Z_{i+m}$ of the results of measurement. But we know functions $\delta_i = f_i(z_1 \ldots z_i \ldots z_n)$ and do not know just the constant coefficients, which enters into these dependences.

Formula (4) describes the standard uncertainty δ_r of the measurement of the real MC:

$$\delta_r = \sqrt{\delta_0^2 + \Sigma_1^j \delta_i^2 + \delta_s^2} \tag{4}$$

To eliminate the influence of the uncertainties $\delta_1 \ldots \delta_i \ldots \delta_j$ on the results of measurement, the variation method was developed (VM) [9]. **Figure 2** illustrates this method. Here, MC contains **n** additional variators $V_1 \ldots V_j$. Last ones influence the uncertainty sources $z_1 \ldots z_j$ and change the uncertainty $\delta_1 \ldots \delta_j$. It creates the output of the proper results of MC measurement $Z_{x1} \ldots Z_{xj}$.

Variators cannot change the uncertainties δ_0 and δ_s. These uncertainties are supposed to be known or equal to zero during the VM calibration.

VM consists of the following steps:

1. First, MC measures initial value Z_{x0} of the input value Z_x.
2. Then, MC consequently varies the influence of the disturbing factor z_i on the well-known value α_i.

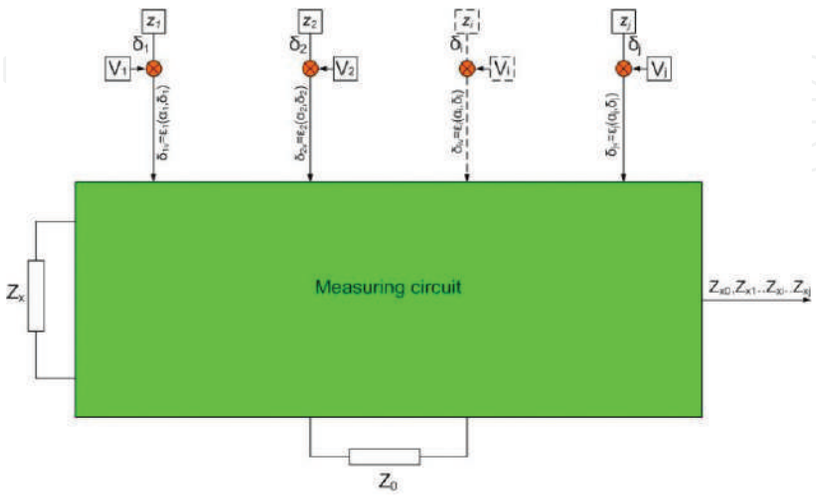

Figure 2. Variational measuring circuit.

Variations could be provided in any order. To simplify the system of equations, it is preferable to perform variations sequentially and to switch ON the variation α_i when all other variations are switched OFF.

Variations could have any law. To simplify the system of equation, it is preferable to provide the multiplicative variation (when we multiply the appropriate uncertainty component δ_i on well-known ratio α_i ($\delta_{iv} = \alpha_i\delta_i$)) or additive variation (when we add the appropriate well-known uncertainty Δ_v to the uncertainty component Δ_{im} ($\Delta_{iv} = \Delta_{im} + \Delta_v$)).

3. After every variation, MC measures the results of the measurement $Z_{x1}\ldots Z_{xi}\ldots Z_{xj}$.
4. The system of Eqs. (5) describes these measurements:

$$\begin{aligned} Z_{x0} &= \gamma\left(Z_x, \delta_1 \ldots \delta_i \ldots \delta_j, \delta_0, \delta_s\right) \\ Z_{x1} &= \gamma\left(Z_x, \delta_1, \alpha_1 \ldots \delta_i \ldots \delta_j, \delta_0, \delta_s\right) \\ Z_{xj} &= \gamma\left(Z_x, \delta_1 \ldots \delta_i \ldots \delta_j, a_j, \delta_0, \delta_s\right) \end{aligned} \tag{5}$$

The system (5) contains j + 1 unknown quantities: Z_x and uncertainties of measurement $\delta_1\ldots\delta_j$, and j + 1 results of measurement $Z_{x0}\ldots Z_{xj}$. Solution (6) of this system gets the true value of the results of measurement Z_x and the values of the uncertainties $\delta_1\ldots\delta_j$ of the measurement:

$$\begin{aligned} Z_x &= \rho_0\left[\left(Z_{x0} - Z_{xj}\right), \left(\alpha_1 - \alpha_j\right), \delta_0, \delta_s\right] \\ \delta_1 &= \rho_1\left[\left(Z_{x0} - Z_{xj}\right), \left(\alpha_1 - \alpha_j\right), \delta_0, \delta_s\right] \\ \delta_j &= \rho_j\left[\left(Z_{x0} - Z_{xj}\right), \left(\alpha_1 - \alpha_j\right), \delta_0, \delta_s\right] \end{aligned} \tag{6}$$

Periodical variation calibration lets us to observe the behavior of every disturbing factor, to determine their stability, to monitor measuring circuit and to ensure precision of the period of the variational calibration.

Let the uncertainty caused by the finite sensitivity of the *i*-measurement be δ_{si} and the uncertainty of the variation α_i be $\delta\alpha_i$. In this case, formula (7) describes the resulting standard uncertainty δ_c of the measurement with variation calibration:

$$\delta_c = \sqrt{\delta_0^2 + \Sigma_0^j\left(\delta_i^2\delta\alpha_i^2 + \delta_{si}^2\right)} \tag{7}$$

Eq. (7) shows that the VM sharply decreases influence of the uncertainty components δ_i on the common uncertainty of measurement (on the $1/\delta\alpha_i$ times).

Let us suppose uncertainty source z_i creates uncertainty $\delta_i = 10^{-3}$ and we need to decrease it to the value 10^{-6}. It means that we have to provide appropriate variation with uncertainty better than 10^{-3} only. It is a very important result of the VM. This effect is restricted only by the stability of the uncertainties $\delta_1\ldots\delta_j$ during the time of measurement.

Let us suppose that time of every measurement is t_i. It means that the common time t_c of measurement increases to the value:

http://dx.doi.org/10.5772/intechopen.74220

$$t_c = \Sigma_0^j t_i \tag{8}$$

Let us suppose that $\delta\alpha_i = 0$ and $\delta_0 = 0$. In this case, formula (9) describes the standard uncertainty of measurement caused by sensitivity of measurements only:

$$\delta_c = \sqrt{\Sigma_0^j \delta_{si}^2}. \tag{9}$$

Formulas (8) and (9) show that the variation method has two disadvantages:

- Variation method needs **n + 1** measurement instead **one** only. It sufficiently increases the time of measurement.
- Variation method increases the contribution of measurement sensitivity δ_{si} in the common uncertainty of measurement.

We can overcome these two disadvantages of the variation method in different ways. Here, we shortly describe *time and space clustering of the thesaurus of the uncertainty sources*.

2.1.1. Time clustering

Usually, different uncertainty sources have different typical speeds of drift. We can divide the thesaurus of **j** uncertainty sources into clusters, which have congruous time of drift. **Figure 3** illustrates this approach. In **Figure 3**, thesaurus of the **j** uncertainty components is divided into three clusters T_1, T_2 and T_3 **(j = m + n + k)**.

The first cluster (T_1) joins ***m*** of the most stable uncertainty sources. It could be instability of the internal standards or arms ratios in transformer bridges, and so on. MC provides their calibration very seldom, for example, one time per year. For this calibration, MC performs sequential

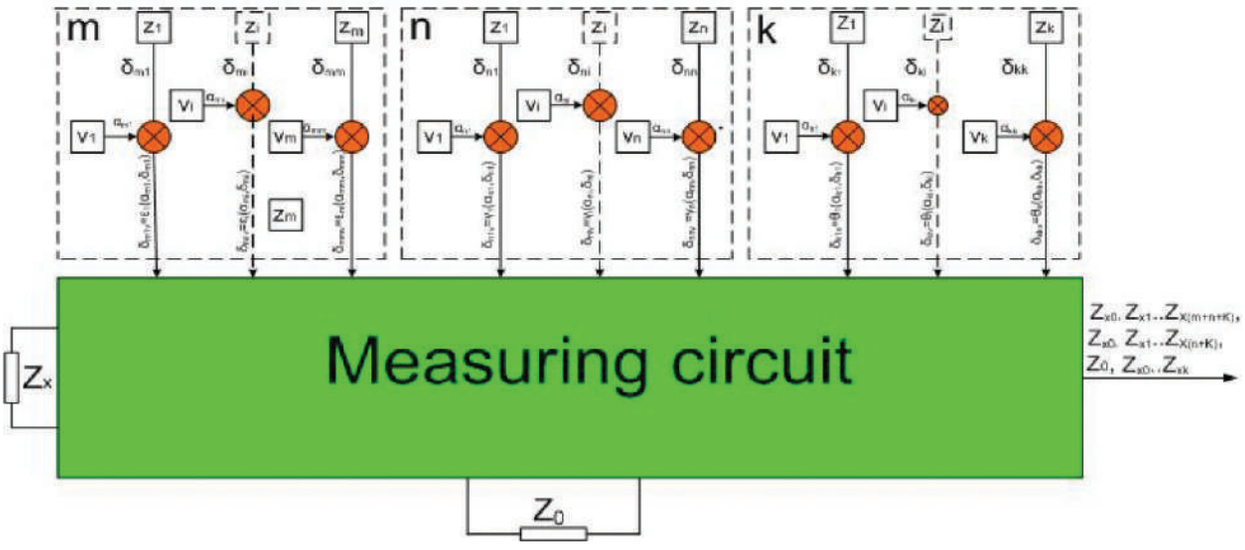

Figure 3. Variation calibration with time clustering.

variation of all sources of uncertainty and provides **m + n + k + 1** measurements. The system (5) of equations describes the results of these measurements. Solution (6) of this system gets us values of the **m** uncertainties of the first cluster.

The second cluster (T_2) joins the **n** less stable sources of the uncertainty. It could be the temperature dependences of the operational amplifiers parameters, and so on. Calibration of these sources is provided more frequently, for example, one time per hour. During this calibration, we suppose that the **m** uncertainties of the first clusters are stable. Values of these uncertainties enter in the system (5) as constants. To find values of the **n** uncertainties of the second cluster, MC varies sequentially the uncertainty sources **n + k**, provides proper measurements and solves the system (5). It needs **n + k + 1** measurements.

The third cluster (T_3) joins the ***k*** uncertainty sources which change most quickly. This cluster mostly includes the sources, which directly depends on the parameters of the object to be measured. This calibration is aimed to find the true results of measurement and values of the last **k** uncertainties. During this calibration, we suppose that uncertainties of the first and second clusters are stable. Their appropriate values are entered in system (5) as constants. Calibration now consists of sequential variation of the **k** uncertainties of third cluster and appropriate measurements. Solution of the system (5) gets us the true results of measurement Z_x and last **k** uncertainties. This calibration needs **k + 1** measurements only.

Let us suppose that any measurement needs time t_i. Formula (10) describes the weighted average t_c of the measurement with variation calibration:

$$t_c = \Sigma_1^k t_i \left(1 + \frac{n+k}{m+n+k}\frac{T_k}{T_m} + \frac{k}{m+n+k}\frac{T_k}{T_m}\right) \tag{10}$$

where $\Sigma_1^k t_i$ is the time of the k cluster calibration and measurement, T_n/T_m is the ratio of the periods of the second T_n and first T_m clusters calibrations and T_k/T_m is the ratio of the periods of the third T_k and first T_m cluster calibrations.

Formula (10) shows that the time of measurement decreases only slightly during the time of calibration of the third cluster. It means sufficient diminution of the time of measurement.

2.1.2. Space clustering

Sometimes, we do not need to separately study every component of the measurement uncertainty. In this case, we use space clustering. During the space clustering, MC is represented as a complex of the **n** quadripoles and standards to be compared. **Figure 4** shows such decomposition of the measurement circuit.

In **Figure 4**, K_1 … K_n are the quadripoles of the MC and the V_1…V_n are the variators used to vary the transfer coefficient of the proper quadripole.

The following formula describes the decomposed MC:

$$Z_{x0} = f(Z_x, K_1, \Delta K_1 \ldots K_i, \Delta K_i \ldots K_n, \Delta K_n) \tag{11}$$

http://dx.doi.org/10.5772/intechopen.74220

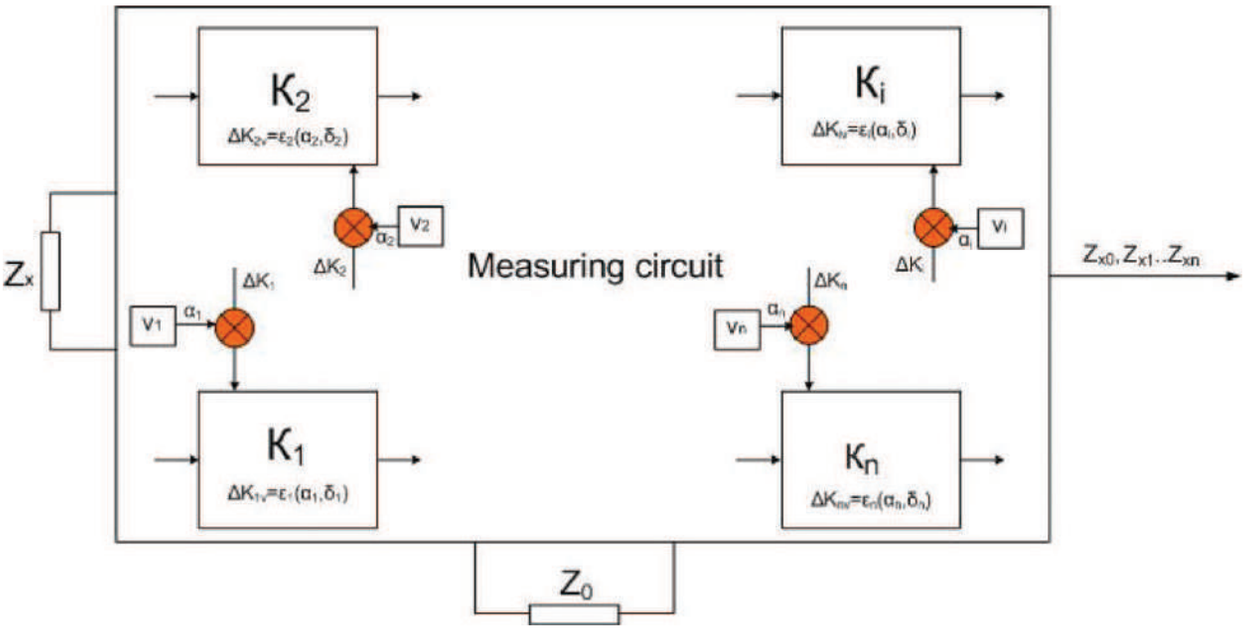

Figure 4. Variation correction with space clustering.

where Z_x and Z_{x0} are the MC input and output values, respectively, $\Delta K_1 \ldots \Delta K_{i\ldots} \Delta K_n$ are the uncertainties of the quadripole transfer coefficients $K_1 \ldots K_i \ldots K_n$.

The following formula expresses the dependence of the measurement uncertainty δ_r on the components of the decomposed MC:

$$\delta_r = \sqrt{\delta_0^2 + \delta_s^2 + \Sigma_1^n \Delta K_i^2} \tag{12}$$

where δ_s is the uncertainty caused by the finite MC sensitivity.

Let us provide **n** well-known variations $v_1 \ldots v_i \ldots v_n$ of the quadripole transfer coefficients $K_1 \ldots K_i \ldots K_n$. MC provides the new measurements $Z_{x0\ldots} Z_{xi} \ldots Z_{xn}$ of the unknown value Z_x after every variation. The system of Eq. (13) describes these measurements:

$$\begin{aligned} Z_{x0} &= f(Z_x, K_1, \Delta K_1 \ldots K_i, \Delta K_i \ldots K_n, \Delta K_n) \\ Z_{x1} &= f(Z_x, K_1, \Delta K_1, v_1 \ldots K_i, \Delta K_i, \ldots K_n, \Delta K_n) \\ Z_{xn} &= f(Z_x, K_1, \Delta K_1 \ldots K_i, \Delta K_i \ldots K_n, \Delta K_n, v_n) \end{aligned} \tag{13}$$

Solution of the system (13) of equations gets accurate results of measurement together with all uncertainties of the quadripoles.

Formulas (8) and (9) describe the uncertainty and time of measurement when using the space clustering as well. However, the number of measurements in case of space clustering is much less. Error accumulation and common time of measurement are much less as well.

We can decompose the measuring circuit in different ways. Optimal decomposition depends on the structure of the measuring circuit. Here, it is impossible to analyze all these possibilities. In most cases, we are forced to use time and space clustering together.

It should be noted that variation method was used earlier in some measurements (e.g., elimination of the uncertainty caused by self-heating of the resistive thermometer in temperature measurements). Here, we consider generalization and dissemination of this method in different areas, first in impedance measurements.

2.2. Experimental developments of the VM

VM was used in several developments. It is too complicated to analyze all these possible applications. Here, we consider only some applications of this method in very important cases of widely used digibridges and in accurate transformer bridges.

2.2.1. Application of the VM in digibridges

Development of the integral operational amplifiers and microprocessors resulted in the new class of measuring devices—digibridges [10–12]. Nowadays, digibridges cover most part of the specific market of the impedance meters. Now many companies manufacture digibridges (HP, Agilent, TeGam, IetLab, Wine Kerr, etc).

2.2.1.1. Operation and analysis

A usual digibridge consists of two serially coupled impedances Z_x and Z_0 (see **Figure 5**) These impedances are connected between outputs of the generator G and the protecting amplifier A. Negative input of this amplifier is connected to the common point of the impedances Z_x and Z_0. Amplifier A creates in this point the potential, close to zero (virtual ground). The same current I_x flows through both impedances Z_x and Z_0 and creates voltages U_x and U_0. Differential vector voltmeter DVV, through switcher S_0, measures these voltages and transfers the

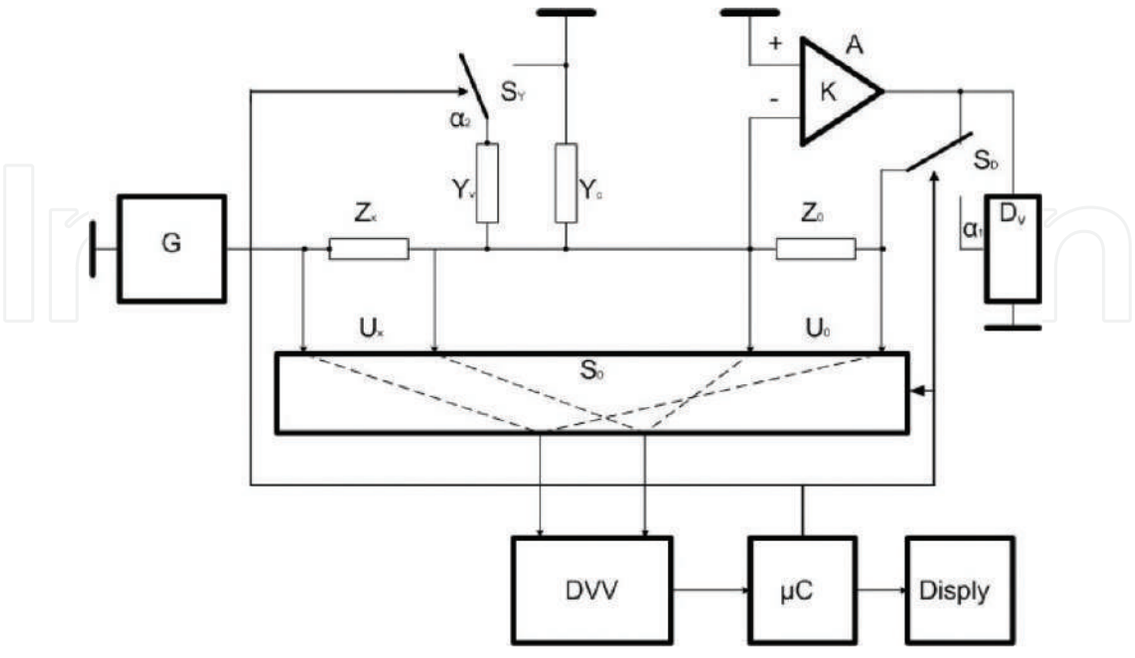

Figure 5. Structure of the digibridge with variational calibration.

http://dx.doi.org/10.5772/intechopen.74220

results of measurement to microcontroller μC. μC controls the operation of the MC, processes results of the voltages measurements and calculates the ratio of two impedances Z_x and $Z_{0.}$ Display D shows results of measurements.

The amplifier A protects measuring circuit and decreases the influence of the parasitic admittance Y_c between the amplifier inputs on the results of measurement.

In case if gain K is infinite, Eq. (14) describes the process of measurement:

$$Z_x/Z_0 = U_x/U_0 \tag{14}$$

Let gain K be finite. In this case, admittance Y_c between the amplifier inputs cause one of the biggest sources of the measurement uncertainty. This uncertainty (δZ) strongly limits the measurements of the high impedances on high frequencies. δZ is described by the equation:

$$\delta Z = Y_c Z_0/(1+K) \tag{15}$$

If K » 1, we can write:

$$\delta Z \cong Y_c Z_0/K \tag{16}$$

Here, the values Y_c and K are the disturbing factors. The quotient of the Y_c and K can be considered as the sole source of the uncertainty. Let us provide the multiplicative variation of the gain K of the amplifier A. To vary K on ratio α_1, the divider D_v with transfer coefficient 1 or α_1 (**Figure 5**) is used. After this variation, MC measures the additional voltage U_{0v}.

The system of three equations describes the measurements of the voltages U_x, U_o and U_{ov}.

$$U_x = I_x Z_x; \quad U_0(1 - Y_c Z_0/K) = I_x Z_0; \quad U_0(1 - Y_c Z_0/K) = I_x Z_0 \tag{17}$$

Solution of this system gets the following formula (18):

$$Z_x/Z_0 = U_x[1 - \delta U \cdot \alpha_1/(1-\alpha_1)]/U_0 \tag{18}$$

where $\delta U = 1 - U_0/U_{0v}$

Analysis of the formula (18) shows that the uncertainty of the variation calibration has minimal if α_1=0.5. Then:

$$Z_x/Z_0 = U_x(1 - \delta U)/U_0 \tag{19}$$

Formula (19) shows that the ratio Z_x/Z_0 does not depend on the quotient of the Y_c and K.

But here increases component of the uncertainty, caused by the increased number of measurements. VV measures quadrature components **a** and **b** of three voltages: U_x, U_o and U_{0v}. Let us suppose that effective input noise of the VV in all these measurement has the same value Δ and the results of measurement are not correlated. In this case, the following formulas are justified:

$$U_x = (a_x + \Delta) + j(b_x + \Delta); U_0 = (a_0 + \Delta) + j(b_0 + \Delta); U_{0v} = (a_{0v} + \Delta) + j(b_x + \Delta) \quad (20)$$

Let us substitute formula (20) in (14) and (19). It gets the following formulas for two cases:

Without variational calibration:

$$\delta_m \approx \sqrt{2}\delta_n \text{ and } \Delta_a \approx \sqrt{2}\delta_n \quad (21)$$

With variational calibration:

$$\delta_m \approx \sqrt{5}\delta_n \text{ and } \Delta_a \approx \sqrt{2}\delta_n \quad (22)$$

where δ_m and Δ_a are the multiplicative and additive uncertainties caused by the relative noise δ_n of the VV.

Formulas (21) and (22) show that the additive uncertainty Δ_a caused by the relative noise ($\delta_n = \Delta/U_0$) in both cases is the same. But these formulas also show that due to the variational calibration, the multiplicative random uncertainty δ_m increases 1.6 times.

Calculation of the uncertainty by the formula (16) has the truncation error δ_t caused by inequality $K \gg 1$ ($\delta_t = Z_0 Y_c/K$). This error sharply increases when K on high frequencies is low, so that calibration practically does not work when $K \to 1$. If amplifier gain K is so low, we cannot consider value Y_c/K as the sole source of the uncertainty. As a result, we have to provide **two** separate variations: multiplicative variation of the gain K and additive variation of the admittance Y_c (using variational admittance Y_v and switcher S_v). DVV measures sequentially voltages U_x, U_0 and $U_0^{'}$, $U_0^{''}$ after multiplicative variation of the gain K and additive variation of the admittance Y_c.

System of three equations describes these four measurements:

$$\begin{aligned} U_x/U_0 &= Z_x/Z_0[1 + Y_c Z_0/(1 + K)] \\ U_x/U_0 &= Z_x/Z_0[1 + Y_c Z_0/(1 + \alpha_1 K)] \\ U_x/U_0 &= Z_x/Z_0[1 + (Y_c + Y_v)Z_0/(1 + K)] \end{aligned} \quad (23)$$

Solution of the system (23) gets following two equations:

$$\begin{aligned} Y_c Z_0 &= \left(A^{'} - 1\right)(\alpha_1 K + 1)(K + 1)/K(1 - \alpha_1) \\ aK^2 &+ bK + c = 0 \end{aligned} \quad (24)$$

here: $a = [(1 + \alpha_1) - \alpha_1(A^{'} - 1)](A^{''} - 1)$, $b = (Y_v Z_o + A^{'})A^{''} - A^{'}$, $c = (A^{'} - 1)(A^{''} - 1)$, $A' = U_0^{'}/U_0$, $A^{''} = U_0^{'}/U_0$

Solution of the Eqs. (24) and substitution of these results in (15) gets the accurate results of measurement which absolutely does not depend on the values Y_c and K.

http://dx.doi.org/10.5772/intechopen.74220

The described approach could be used for the accurate calibration of any amplifier with positive or negative gain, followers, gyrators, and so on. It could be used for calibration of any control system as well.

3. Experimental results

The earlier described approach was used in digibridge MNS1200. This digibridge was developed for Siberian Institute of Metrology (Novosibirsk), to be used in working inductance standard. Its short specification is as follows.

MNS1200 operates in frequency range of DC to 1 MHz.

Frequency set discreteness 2×10^{-5}.

Capacitance range of measurement (F) 10^{-17}–10^{5}.

Resistance range of measurement (R) 10^{-6}–10^{14}.

Inductance range of measurement (H) 10^{-12}–10^{10}.

Dissipation factor tgδ (tgφ) 10^{-6}–1.0.

Main uncertainty (ppm) 10.

Sensitivity (ppm) 0.5

Inner standard instability (24 hours, ppm) ± 2.

Weight (kg) 4

MNS1200 appearance is shown in **Figure 6**.

Instability of the MNS1200 inner standard can achieve 10^{-4} in a long period of time. To get maximal accuracy, MNS1200 can be calibrated by arbitrary R,L,C outer standard. In this case,

Figure 6. Digibridge MNS1200.

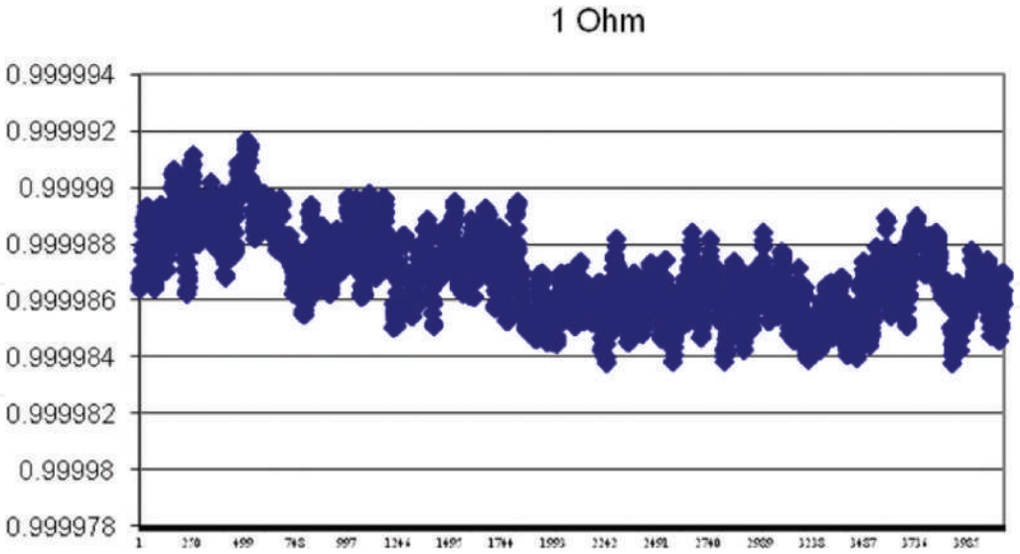

Figure 7. Results of the 24-hour 1 Ohm standard measurements.

uncertainty of measurement depends on short-time stability of inner standards. Results of the 24-hour 1 Ohm standard measurements are shown in **Figure 7**.

3.1. Application of the VM in transformer bridge

Accurate comparison and unit dissemination of the impedance parameters are provided using many different, very complicated manual bridges with numerous different standards. The main world-renowned laboratories (BIPM, NIST, NML, NPL, PTB, VNIIM, etc.) in developed countries have their own primary standards, based on the calculable capacitor [13, 14] and the appropriate transformer bridges [15, 16], on the quantum hall resistance [17] and the appropriate bridges [18, 19] and very accurate quadrature transformer bridges for comparison of different impedance parameters [20, 21], that have original constructions. All these bridges contain complicated set of devices and have long and intricate handle balancing processes. In addition, these bridges and standards are of different kinds and are located in various laboratories. The process of calibration and traceability is, therefore, complicated and very expensive. Uncertainty of the measurement of these bridges achieves 10^{-8}–10^{-9}. It makes them an excellent instrument for fundamental investigations.

For practical needs of the metrologic calibration, it is enough to provide measurements with uncertainty about 10^{-6}. In this case, the equipment have to be universal, to compare arbitrary standards, to have low cost and weight and to be transportable. The complex of bridges described later satisfies these demands. Complex consists of autotransformer and quadrature bridges. Both of them are based on the variational calibration. Autotransformer bridge provides unit transfers in the whole range of the impedance of the C,L,R standards. Quadrature bridge provides cross transfers of the units. Last bridge is described in [22, 23].

This chapter describes the part of the results of this project, covering the development of the transformer bridge-comparators which transfer units of the resistance, inductance, capacitance

http://dx.doi.org/10.5772/intechopen.74220

and dissipation factor in a whole range of measurements and reciprocal transfer of any units. Balance and calibration of these bridges are based on the variational method.

3.1.1. Autotransformer bridge: description and analysis

Early autotransformer bridges were described in [24, 25]. These bridges have been widely used up to now [15, 16]. To eliminate the influence of the cable impedance (yoke) on the results of measurement, double autotransformer bridges are used [3, 5]. The wide-range double autotransformer bridge contains two inductive dividers, simultaneously controlled for bridge balance. For accurate measurements, these inductive dividers usually are of a two-stage design at least. Every stage of these inductive dividers [26] consists of a lot of turns and appropriate complicate switchers. They have to have multidigit capacity (up to seven or eight digits). This quite complicates the bridge.

Development of the variational bridge has to solve two problems:

- to eliminate the Yoke (Z_n) influence on the results of measurement without using the double autotransformer bridge;
- to decrease sharply the number of the autotransformer divider decades without loss in the accuracy of measurement.

The simplified measuring circuit of the automatic variational bridge (PICS) [27], which solves these problems, is shown in **Figure 8**.

The bridge consists of the supply unit (the generator G connected to the voltage transformer TV), the main autotransformer AT and the variationally balanced 90° phase shifter [28], which is calibrated through calibration circuit CC. The vector voltmeter VV (through the preamplifier PA and switchers S_1 and S_2) measures the bridge (U_1, U_2) and the calibration circuit CC (U_c)

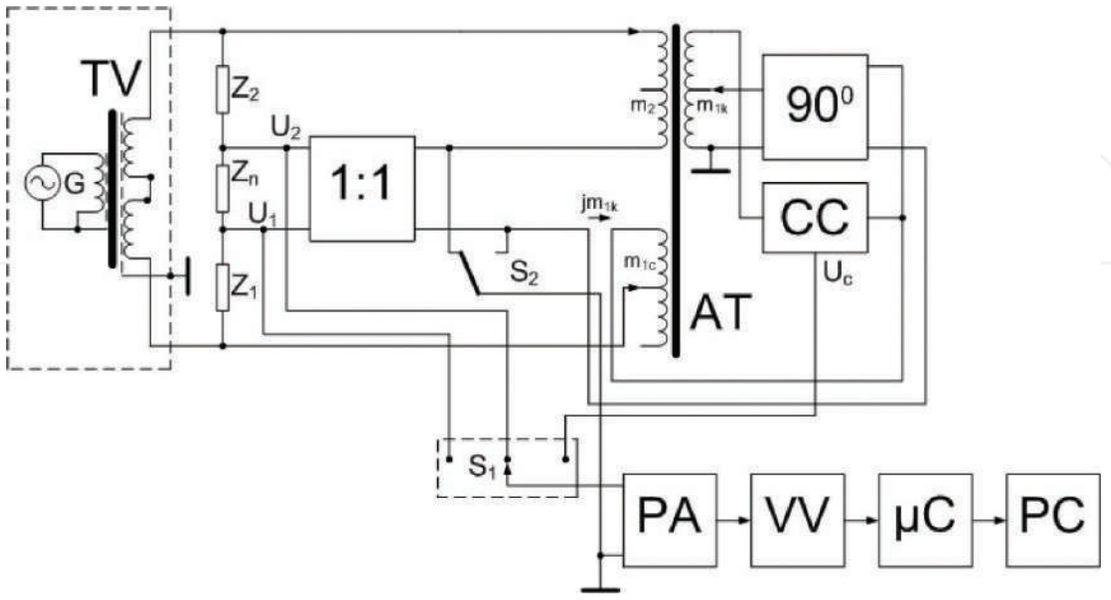

Figure 8. Circuit diagram of the autotransformer bridge.

unbalances the signals. The differential voltage follower 1:1 compensates the voltage drop U_n on the cable impedance Z_n. The microcontroller μC transfers the results of the VV measurements to the personal computer PC and controls the bridge balance and calibration of the phase shifter 90°. The autotransformer AT Carries on its core windings m_2, m_{1c} and m_{1k}. These windings are used to balance the bridge by the main (m_{1c}) and secondary (m_{1k}) parameters. The standards to be compared Z_1 and Z_2 are connected serially by the cable (yoke) and by their high potential ports, to voltage transformer TV and to the windings m_{1c} and m_2 of the autotransformer AT.

The output of the 90° phase shifter is connected in series with the winding m_{1c} to create the balance winding $m_1 = m_{1c} + jm_{1k}$.

The drop of the voltage U_n acts on the impedance Z_n of the cable which connects Z_1 and Z_2. This voltage is applied to the input of the differential voltage follower 1:1.

The two-channel VV has two digital synchronous demodulators, proper LF digital filters and Σ-Δ ADC. It simultaneously measures two orthogonal components of the bridge unbalance signals. This voltmeter has high selectivity (equivalent Q-factor is higher than 10^5). Its integral nonlinearity is better than 10^{-4} and relative sensitivity is better than 10^{-5}. The VV is calibrated automatically and periodically by variational algorithm, described in [29].

On the low impedance ranges, the drop U_n of the voltage on the cable impedance increases. This increases the uncertainty of the bridge unbalance measurement. To decrease this effect, the voltage follower 1:1 is used. This follower places the named drop of the voltage between low potential pins of the windings m_1 and m_2. It decreases the effective cable impedance from Z_n to the equivalent value $Z_{ne} = Z_n\delta$, where δ is the uncertainty of the transfer coefficient of the voltage follower.

To decrease the number of the decades of the autotransformer divider and eliminate the influence of the Z_n on the results of measurement, the bridge operates in a non-fully balance mode and use twice variational balance [27].

In compliance with developed variational algorithm, VV measures sequentially the bridge unbalance signals U_1 and U_2. After that, μC varies the turns of the winding m_1 on Δm_v and VV measures the variational signal U_{2v}.

The system of Eqs. (30) describes these three measurements:

$$\begin{aligned} &U_0(Z_1/Z_c) - U_0[1 - Z_n(1+\delta)/Z_c]m_1/(m_1+m_2) - U_1 = 0 \\ &-U_0[1 - Z_n(1+\delta)/Z_c]m_2/(m_1+m_2) + U_0Z_2/Z_c + U_2 = 0 \\ &-U_0[1 - Z_n(1+\delta)/Z_c]m_2/(m_1+m_2+\Delta m_v) + U_0Z_2/Z_c + U_{2v} = 0 \end{aligned} \tag{25}$$

where $Z_c = Z_1 + Z_2 + Z_n$, and δ is the uncertainty of the voltage follower 1:1, U_0 is the supply voltage.

The formula (26) gives the solution of the system (25):

$$\delta Z = -\frac{\delta_v}{2}\frac{m_1+m_2}{m_2}\left(C + \frac{m_1-m_2}{m_1+m_2}D\right)/[1 + (C+D)\delta_v] \tag{26}$$

where

http://dx.doi.org/10.5772/intechopen.74220

$$C = (U_2 + U_1)/(U_{2v} - U_2); D = (U_2 - U_1)/(U_{2v} - U_2); \delta_v = \delta m/(1 + \delta m); \delta m = \Delta m_v/(m_1 + m_2)$$

μC uses the results of the calculation of the bridge unbalance δZ_c by described algorithm in two stages:

- in the first stage, μC makes quick, automatic balance of the bridge on the four high-order decades (balance stage);
- in the second stage, μC increases the sensitivity of the voltmeter VV on 10^4 and decreases the value of the variation Δm_v of the m_1 turns in the same ratio. Then, μC repeats the measurements by described algorithm. Results of these measurements and calculations by formula (26) determine the balance point coordinates and find the impedance ratio:

$$\frac{Z_1}{Z_2} = \frac{m_1}{m_2} - \delta Z \tag{27}$$

The final result is given in 8.5 digits.

The bridge balance and data processing by described variational algorithm reduce the number of the autotransformer dividers to only one and sharply (twice) reduce the number of the digits of this divider.

The 90° phase shifter and the calibration circuit CC **do not contain accurate internal standards** of capacitance or resistance. To get good accuracy, we use the special phase shifter calibration procedure based on the variational method. Simplified structure of this phase shifter is shown in **Figure 9**.

Phase shifter consists of serially connected inverter I and proper phase shifter PS. Firstly, calibrating circuit (resistors R_1 and R_2) and switchers S_1 and S_2 are used to calibrate inverter I. Secondly, calibrating circuit (resistor R_1 and capacitor C_1) and switchers S_3 and S_4 are used to calibrate the phase shifter PS. Vector voltmeter VV, through switcher S_5 measures unbalance signals of the first or second calibration circuits and translates the results of measurements to microcontroller μC. Finally, one controls all calibration procedure and calculates PS real transfer coefficient.

Calibration procedure consists of two stages.

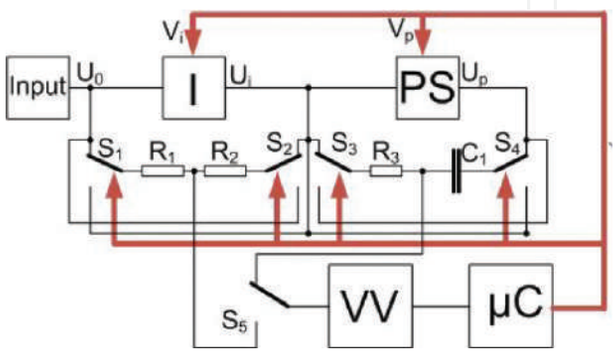

Figure 9. Structure of the phase shifter.

4. Calibration of the inverter I

To calibrate the inverter, the VV measures three signals of the calibration circuit R_1–R_2:

- The initial output signal of the calibration circuit U_{i1};
- The signal U_{i2} after the variation of the inverter transfer coefficient on the value δ_{iv};
- The signal U_{i3} after the inversion of the connection of the calibration circuit between the input and output of the inverter I by the switchers S_1 and S_2.

Complex of these signals is described by proper system of equations. Solution of this system (formula 38) gets the accurate deviation δ_i of the inverter transfer coefficient from its nominal value "1."

$$\delta_i = \delta_{ia}(1 + \delta_{kia}) \tag{28}$$

where.

$\delta_{ia} \approx \frac{\delta_{iv}}{2}\frac{U_{i3}+U_{i1}}{U_{i2}-U_{i1}}$; $\delta_{kia} \approx \frac{\delta_{iv}}{2}\frac{U_{i3}-U_{i1}}{U_{i2}-U_{i1}}$; δ_{ia} and δ_{kia} are the approximate values of the transfer coefficients of the inverter I and calibration circuit R_1-R_2.

5. Calibration of the phase shifter PS

To calibrate the phase shifter PS, the VV measures three signals of the calibration circuit R_3-C_1:

- The initial output signal U_{p1} of the calibration circuit, when calibration circuit is connected between input and output of the phase shifter;
- The signal U_{p2} after the variation of the phase shifter PS transfer coefficient in the value δ_{pv};
- The signal U_{p3} after the inversion of the calibration circuit and connection of this circuit between the input of the inverter I and output of the phase shifter PS by the switchers S_1 and S_2.

Complex of these signals is described by proper system of equations. Solution of this system (formula (29)) gets the accurate deviation δ_p of the phase shifter PS transfer coefficient from its nominal value "j":

$$\delta_p = \delta_{pa}\left(1 + \delta_{kpa}\right) \tag{29}$$

where:

$$\delta_{pa} \approx \frac{\delta_{pv}}{2}\frac{jU_{p3} + U_{p1}}{U_{p2} - U_{p1}} - \frac{\delta_i}{2}\frac{1}{1+\delta_i} \text{ and}$$

$$\delta_{kpa} \approx \frac{\delta_{pv}}{2}\frac{jU_{p3} - U_{p1}}{U_{p2} - U_{p1}} - \frac{\delta_i}{2}\frac{1}{1+\delta_i}$$

δ_{pa} and δ_{pka} are the approximate values of the transfer coefficients of the inverter PS and calibration circuit, respectively.

http://dx.doi.org/10.5772/intechopen.74220

After the calibration procedure, we know the real value of the phase shifter transfer coefficient with an uncertainty better than 1–3 ppm. μC makes this calibration procedure automatically at least every hour.

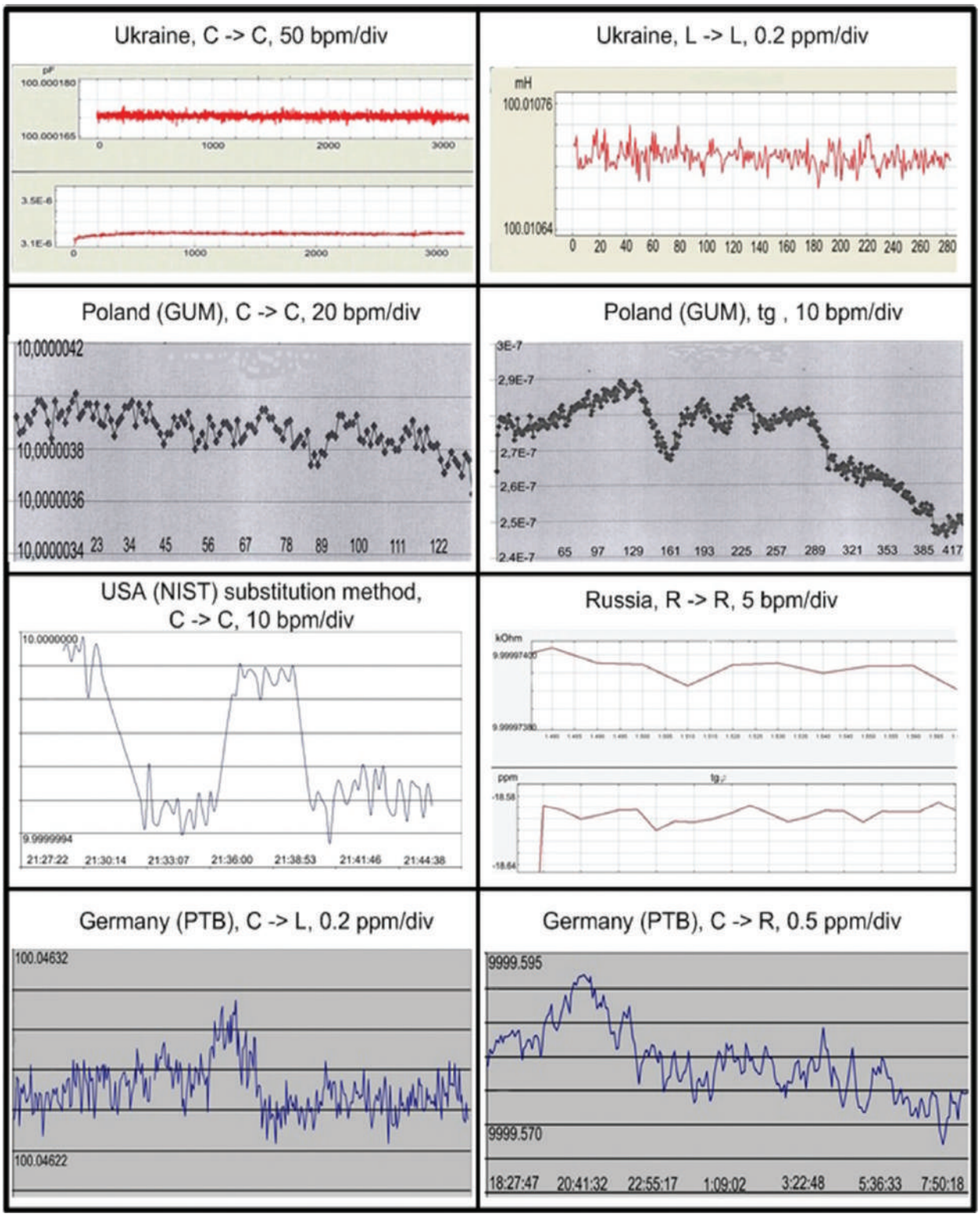

Figure 10. Some results of experimental investigations.

5.1. Experimental results

All results of the theoretical investigations shown earlier were used to develop the comparator PICS.

PICS very short specification is given as follows.

Short PICS Specification.

PICS operates on frequencies 1.00 and 1.59 kHz.

Frequency set discreteness 5×10^{-5}.

Capacitance range of measurement (F) 10^{-19}–10^{-3}.

Resistance range of measurement (R) 10^{-7}–10^{8}.

Inductance range of measurement (H) 10^{-12}–10^{3}.

Dissipation factor tgδ (tgφ) 10^{-6}–1.0.

Main uncertainty (ppm) 1.0.

Sensitivity (ppm) 0.02–0.05

Weight (kg) 5

PICS was tested in USA (NIST) and Russia (VNIIM), in Germany (PTB) and Poland (GUM), in Ukraine (Ukrmetrteststandard) and Byalorussia (Center of metrology).

Some results of these tests are shown in **Figure 10**.

Appearance of the PICS, together with intermediary thermostated standards, is shown in **Figure 11**.

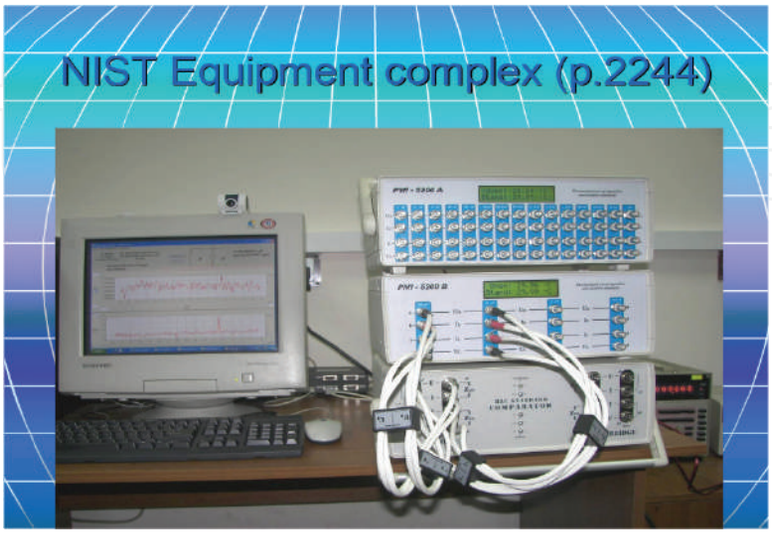

Figure 11. Appearance of the PICS.

http://dx.doi.org/10.5772/intechopen.74220

6. Conclusion

Variational calibration sharply increases the accuracy of measurement. In case of variation correction, for precision measurements, we can use simple and cheap measuring circuits with rather high uncertainty. Variational calibration diminishes the uncertainty of such circuits on thousands or even more times. It does not need too accurate variational standards. Time and space clustering in significant measure overcomes disadvantages of this calibration—increasing the time of measurement. Experimental investigations of the comparator PICS have shown that uncertainty of measurement on main ranges is lower than 10^{-6} and sensitivity is better than 10^{-7}–10^{-8}. Variational calibration also decreases the weight and cost of the accurate equipment.

Acknowledgements

The author is grateful to Dr. H. Bachmair, Dr. J. Melcher and Dr. M. Klonz (PTB), to Dr. A. Koffman, Dr. J. Kinnard and Dr. Y. Wang (NIST), to Dr. A. Tarlowski (GUM) for their constant support and very useful advice during the project development, to Dr. H. Hall for his very helpful criticism and advice during paper consideration. I would like to specially acknowledge my teacher F. B. Grinevich and colleagues A. Lameko and D. Surdu, who have spent a great part of their life realizing variational ideas.

Author details

Michael Surdu

Address all correspondence to: michaelsurdu1941@gmail.com

Ukrainian Academy of Metrology, Kiev, Ukraine

References

[1] Hall HP. A History of Z Measurement. 64 pp. www.ietlabs.com/pdf/GenRad_History/A_History_of_Z_Measurement.pdf

[2] Ornatsky PP. Automatic Measurements and Instrumentation. Kiev: High School; 1986. p. 310

[3] Kibble BP, Rayner GH. Coaxial AC Bridges. Bristol: Adam Hilger Ltd; 1984. p. 203

[4] Hague B. Alternating Current Bridge Methods. 6th ed. Pitman Publishing; 1971. p. 602

[5] Grinevich FB. Automatic bridges – Novosibirsk. 216 pp. 1964

[6] Kneller JV, Agamalov JR, Desova AA. Automatic impedance bridges with coordinated balance., S.Pt. Energy. 1975:168

[7] Bromberg EM, Kulikovsky KL. Testing methods of the improvement of the accuracy of measurement. Energy, Moskow. 1978:176 pp

[8] Zemmelman MA. Automatic correction of the uncertainty of measurement. Moskow: Standards publishing house; 1972. 200 pp

[9] Grinevich FB, Surdu MN. precision AC variational measuring systems. Kiev: Scientific thinks; 1989. p. 192

[10] Karandeev KB, and all. Quick-acting electronically balanced measuring systems. Kiev-Moskow. Energy. 1978:134 pp

[11] Maeda K, Narimatsu Y. Multy-frequency LCR meter test components under realistic conditions. Hewlett-Packard Journal. February, 1979;**30**(2):24-32

[12] Hall HP. Method of and Apparatus for Automatic Measurement of Impedance or other Parameters with Microprocessor Calculation Techniques. Pat. USA, No 4196475. 1.04; 1980

[13] Thompson AM, Lampard DG. A new theorem in electrostatic and its application to calculable standard of capacitance. Nature. 1956;**177**:888

[14] Fletcher N. The BIPM/NMIA Calculable Capacitor Project. Conference on Precision Electromagnetic Measurements, June 13–18, 2010, Daejeon, Korea. pp. 318-319

[15] Jeffery AM, Shields J, Shields S, Lee LH. New multi-frequency Bridge at NIST, BNM-LCIE, pp. G1-G37. 1998

[16] Delahaye F. AC-bridges at BIMP. BNM-LCIE. pp.C1-C6. 1998

[17] Klitzing v K, Dorda G, Pepper M. New method for high-accuracy determination of the fine-structure constant based on quantized hall resistance. Physical Review Letters. 1980;**45**:494

[18] Fletcher NE, Williams JM, Janssen A. Cryogenic current comparator resistance ratio bridge for the range 10 kΩ to 1 GΩ. Precision Electromagnetic Measurements Digest, CPEM2000 y. 482-483 pp. 2000

[19] MI6800A – Quantum Hall System, technical description

[20] Thompson AM. An absolute determination of resistance based on calculable standard of capacitance. Metrologia. January 1969;**4**(16):1-7

[21] Trapon G, Thevenot O, Lacueille JC, Poirier W. Determination of the von Klitzing constant R_K in terms of the BNM calculable capacitor - fifteen years of investigations. Metrologia. August 2003;**40**(4):159-171

[22] Surdu M, Lameko A, Surdu D, Kursin S. Wide frequency range quadrature bridge comparator. 16 International Congress of Metrology, Paris, 7–10 Okt, 2013

[23] Surdu M, Kinard J, Koffman A, et al. Theoretical basis of variational quadrature bridge design of alternative current. Moscow, Measurement Techniques. 2006;**10**:58-64

[24] Blumlein AD. British Patent No. 323,037. Alternating Bridge circuits

[25] Wenner F. Methods, apparatus, and procedure for the comparison of precision standard resistors. NBS Research Paper RP1323. NBS Journal of Research. 1940;**25**(Aug):231

[26] Brooks HD, Holtz FC. The two-stage current transformer. Transactions of the American Institute of Electrical Engineers. 1922;**XLI**:382-393

[27] Surdu M, Lameko A, Surdu D, Kursin S. An automatic bridge for the comparison of the impedance standards. Measurement. 2013;**46**:3701-3707

[28] Surdu M, Lameko A, Surdu D, Kursin S. Balanced wide frequency range quadrature phase shifter. Conference on Precision Electromagnetic Measurements CPEM2010, Daejeon, Korea, 6–10 July, 2010

[29] Surdu M et al. Peculiarities of the calibration of the two channel vector voltmeter for the digital AC bridge. UMJ. 2011;**1**:25-30

IntechOpen

Chapter 4

Measuring 'Big G', the Newtonian Constant, with a Frequency Metrology Approach

Andrea De Marchi

Additional information is available at the end of the chapter

http://dx.doi.org/10.5772/intechopen.75635

Abstract

A new approach is described and discussed to the determination of the Newtonian gravitational constant G, which is based on the very powerful measurement of the frequency difference between two similar oscillators. The rate of change of time delay between the two is equal to their relative frequency difference, and small variations of either one can then be detected via delay monitoring with resolution limited only by time resolution and frequency stability of the two oscillators. The latter should be highly sensitive to gravitational field, to measure *G*, which triggers the choice of simple pendulums as field detectors. Since the relative effect on frequency readily obtainable in the lab by well-controlled variations of the gravitational field is on the order of 10^{-7}, stabilities on the order of 10^{-12} are needed of the relative frequency difference if measurement of the fifth decimal digit of *G* is the target of the experiment. It is argued that such high stability is possible with a pendulum properly designed for being locally isochronous and showing an adequately high *Q* factor. The latter is projected to reach possibly 10^7 or more with the discussed design.

Keywords: Newtonian constant, simple pendulum, pendulum frequency stability, time stability, isochronous pendulum

1. Introduction

The presently official value of the Newtonian constant *G* is listed in the most recent CODATA report (2014) as $6.674\ 08 \times 10^{-11}\ m^3\ kg^{-1}\ s^{-2}$, with a quoted relative uncertainty of 4.7×10^{-5}, which still makes it the least well known of all constants of nature, despite improvements derived from a flurry of efforts undertaken in the last decades.

Several different approaches have been followed in the realization of experiments aimed at its determination. A short summary can be found in the introduction of [1], where the experiment illustrated in this chapter was proposed, and for a deeper insight, a well-done recent comprehensive review [2] can be used for reference and comparison. It makes metrological sense to devise different experiments for the purpose, so that the set of possible systematic errors be not the same for all and the risk of undetected coherent biases among various G determinations be minimized. While refurbished and modernized versions of the original Cavendish torsion balance are still the most commonly adopted sensing device and at least one of them has demonstrated extremely high accuracy [3], experiments based on other configurations have also been developed, and a few of them have yielded some of the best results to date. The latter include a measurement based on a beam balance [4] and one based on a pair of simple pendulums used in the static mode [5]. Both achieved accuracy in the low 10^{-5} region. These three determinations of G agree within their stated uncertainty and are the most influential in the 2014 CODATA value, which, however, was attributed higher uncertainty due to the excessive disagreement of other results. A coordinate effort is being led by the recently established working group WG13 of UIAP, stimulated by a NIST initiative, aimed at improving the status of G metrology. The experiments coordinated in this effort are mainly based on the torsion balance approach because of its favorable S/N ratio, hoping to put to fruition the enormous amount of information on systematics affecting it, with the target of improving accuracy by possibly an order of magnitude. However, other approaches are also encouraged, and experiments based differently are monitored or even supported. The free-fall gravimeter [6–8] still appears very promising due to its unique absence of difficult-to-evaluate systematics, but results are still hard to come by, mainly due to the inherently low S/N ratio of these experiments. The experiment presented in this chapter is supported by NIST through its Precision Measurements Grant Program and is based on the adoption of a pair of simple pendulums as a detection device. The target is the determination of G with an accuracy of 10^{-5}. The concept of the experiment has evolved from a pilot experiment carried on at Politecnico di Torino from 1998 to 2005, which used a single pendulum in vacuum and yielded preliminary results at 3% accuracy level [9–11].

2. The dynamic dual simple-pendulum approach

The experiment illustrated here is based on a high-resolution technique, well known in frequency metrology [12], to measure very accurately small frequency differences between two almost synchronous sources. In fact, such small differences Δv produce a variable time delay between the two waveforms, which add up to a full cycle in a time interval $1/\Delta v$. The rate of change of the time delay yields directly the relative frequency difference.

Simple pendulums appear attractive for a G measurement based on this approach, because their small oscillation resonance frequency is directly proportional to the square root of the Earth's gravitational acceleration g, as is well known, which makes them particularly sensitive to a gravitational field variation induced in a controlled way by a displacement of field masses. We will call y the relative frequency change produced in this way. Resolution in this measurement is limited only by time delay resolution and differential frequency stability of

the two sources. For example, if time resolution is 1 ns, a 1000 s run allows to determine the relative frequency difference to 10^{-12}, provided its stability is adequate. This means that the two frequencies can wander around in parallel by more than that but their difference should not. This is important in considering the use of pendulum oscillators, because the gravity acceleration g is not constant in time due to a variety of causes, and so will be their frequency, which will then show instabilities not much below the 10^{-7} level [13]. Nevertheless, since such instabilities affect in a similar way all pendulum oscillators, particularly if they are in the same location, it can be expected to be quite possible that the differential instability of two equal pendulums oscillating not far from each other may be adequate for the projected resolution of the experiment under discussion.

In **Figure 1**, a sketch is shown of the expected evolution of time delay as the active field mass distribution is shifted back and forth between a geometrical configuration in which it increases the frequency of one pendulum and another antisymmetric one in which it increases the frequency of the other one. Suppose one pendulum is slightly slower than the other one (it always will be the case as two exactly equal lengths are very unlikely and even undesirable to avoid coupling). As time goes by, this slower oscillator will show increasing time delay with respect to the other, as indicated in **Figure 1** by the broken trend line. Now, when its frequency is increased by the field masses, it will get closer to that of the faster one, and its time delay rate of change (*DROC*) will decrease. The opposite will happen when the field masses increase the frequency of the other pendulum. The relevant information in this measurement is the difference between *DROC*s in the two configurations.

If v_{s0} and v_{f0} are the undisturbed frequencies of slow and fast pendulums ($v_{f0} - v_{s0} = \Delta v_0 > 0$), their difference will be modified by field masses as in Eq. (1) below, when the latter are next to the slow pendulum, and as in Eq. (2) when they are next to the fast one.

$$\Delta\nu|_s = \nu_{f0}\left(1 + y_{far}\right) - \nu_{s0}(1 + y_{near}) \tag{1}$$

$$\Delta\nu|_f = \nu_{f0}(1 + y_{near}) - \nu_{s0}\left(1 + y_{far}\right) \tag{2}$$

The DROC measurement is performed by measuring the time delay accumulated in n periods of the slow pendulum and dividing it by nT_s, as illustrated in **Figure 2**.

Therefore, it turns out that the relationship between measured DROC and actual frequencies of the two oscillators is.

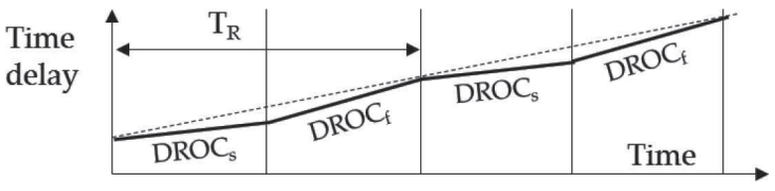

Figure 1. Time delay slope changes as field masses are moved back and forth between the two pendulums with repetition period T_R.

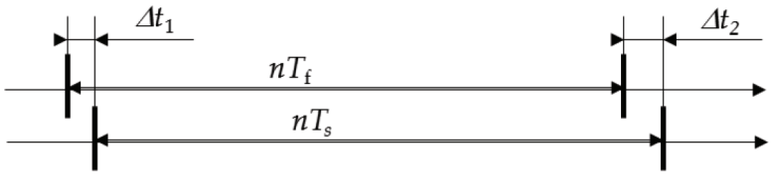

Figure 2. Measurement scheme of the *DROC* (time delay rate of change).

$$DROC = \frac{\Delta t_2 - \Delta t_1}{nT_s} = \frac{n(T_s - T_f)}{nT_s} = \frac{\Delta \nu}{\nu_f}, \tag{3}$$

and the difference between DROCs in the two configurations is then given by.

$$DROC_f - DROC_s = \frac{\nu_{f0} + \nu_{s0}}{\nu_f}\left(y_{near} - y_{far}\right) \approx \left(2 - \frac{\Delta \nu_0}{\nu_f}\right) KG \tag{4}$$

In Eq. (4), the concept was introduced that relative frequency variations induced on pendulums by the field masses are proportional to the Newtonian constant *G* through a proportionality factor *K*. The analysis needed to identify the value of *K* is sketched in the next section. The value of G can be obtained by inverting Eq. (4) and is.

$$G = \frac{DROC_f - DROC_s}{K\left(2 - \frac{\Delta \nu_0}{\nu_f}\right)}. \tag{5}$$

Clearly, *K* must be known with relative uncertainty smaller than the 10^{-5} target *G* accuracy of this experiment. In fact, this may well be the ultimate accuracy limit of this approach.

As for measurement resolution, it is also shown in the next section that the relative effect on pendulum frequency obtainable by a geometrical change in mass distribution around the bob can be on the order of 10^{-7}. It appears therefore clear that a target differential frequency stability of at least 10^{-12} should be looked for in designing the two oscillators. Other than that, the requirements for time interval measurement resolution are instead benign, both because the S/N ratio of pendulum signals is expected to be quite good (more on this in the following) and because the DROC type A uncertainty can be expected to improve as the averaging time to the power 3/2, much faster than the typical power ½ of averaging on white noise [1]. The intuitive explanation for this is in the fact that a linear regression on the scatterplot of delay data versus time will in fact yield a statistical uncertainty improving as the square root of the number of measurements (which is proportional to time), but then the result is divided by elapsed time to get the DROC, which produces the power 3/2 improvement law.

3. Field mass configuration

For the calculation of the gravitational effect on frequency, the relative extra acceleration a_M given to the bob by the system of field masses is the relevant parameter. In fact, for small

oscillations of the bob along x, its angular frequency is given by the square root of $(a_g + a_M)/x$, with $a_g = gx/L$. The relative frequency change y induced by field masses will then be $(a_M/a_g)/2$. A peculiarity of the experiment discussed here, with field masses centered on both sides of the bob, is that both a_g and a_M vanish at rest position, but their ratio does not, as both are linear in x for small displacements. This fact gives this scheme a great advantage over other approaches, because it maximizes the effect exactly where field masses are closest to sensors. For example, this is not the case for free-fall experiments, which see the effect vanish along with a_M where the sensing object spends most of its time, at the apogee of its parabolic flight.

An analysis of the arrangement under discussion, with two equal masses symmetrically centered on either side of the bob rest position, yields for the effect on pendulum frequency.

$$y = \frac{\rho_M}{\rho_E}\frac{L}{R_E}\left(\frac{R}{a}\right)^2 \Gamma(0) \ , \tag{6}$$

where L is the pendulum length, R and a are radius and half distance of field masses between centers, R_E is the Earth's radius, and shown densities are those of the Earth and field masses. $\Gamma(0)$ is the value at $x = 0$ of a geometrical shape factor which is discussed below. It is interesting to point out in Eq. (6) that only the density of field masses is relevant for the size of the effect and not their total mass, other than in the fact that, for a given gap between them, the ratio R/a depends slightly on mass size. Also interesting is to notice that, other than hidden in the size of the gap that must host it, the test mass (which is the bob) does not appear in Eq. (6). This is because neither gravitational acceleration in play, from the Earth or from field masses, depends in any way on the mass of the bob.

The shift of Eq. (6) is expected for small oscillations. However, neither acceleration is strictly linear, which yields the well-known non-isochronism of the simple pendulum plus, relevant for this experiment, a nontrivial tie with the extra gravitational pull. So, while it is easy to find frequency and shift for small oscillations, as the relative extra acceleration can then be considered constant over the swing, nontrivial calculations are necessary for wider swings.

The field masses adopted for the experiment are cylinders of heavy metal positioned, for the "near" configuration, at either side of the bob as shown in **Figure 3a**. The metal could be platinum or, more cheaply, tungsten, but copper is chosen for budget reasons in the preliminary phases. The reason for adopting a cylindrical shape lies in the much higher uniformity of the additional recalling acceleration provided by this shape to a bob displaced from the rest point, with respect to the case of a spherical field mass shape. In **Figure 3b** a plot is given of such additional acceleration (relative to a_g) versus bob displacement in a 1 m pendulum, calculated for two tungsten field masses 85 mm in diameter and 117 mm long, spaced by an 8 mm gap to host a 5 mm spherical bob in between.

The resulting fractional frequency increase y_{near} can be calculated with a suitable integration, which is quite straightforward for oscillation amplitudes not exceeding the uniformity region. The expression of $\Gamma(x)$ used in **Figure 3b**, written with $\eta = w/a$ and $\xi = x/a$, is.

$$\Gamma(x) = \frac{3}{4}\frac{a}{R\xi}\left(\frac{1}{\sqrt{1+(\eta-\xi)^2}} - \frac{1}{\sqrt{1+(\eta+\xi)^2}}\right) \ , \tag{7}$$

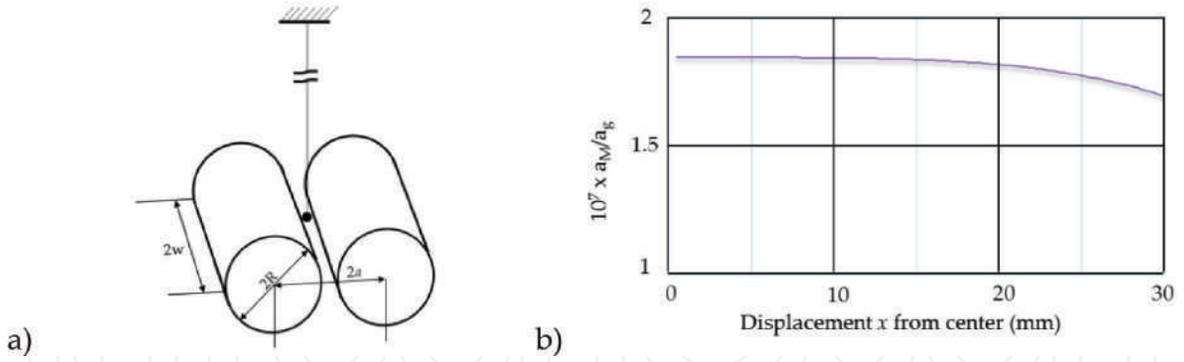

Figure 3. (a) Sketch of the near arrangement of two cylindrical field masses and (b) variations along x, elongation of the bob from rest position, of the recall acceleration a_M produced by the two field masses divided by the relevant g component a_g.

It should be pointed out here that shape factor of the cylindrical field masses was chosen in this calculation to optimize the uniformity of the effect, as shown in **Figure 3b**. The absolute dimension of the masses, instead, was designed to best fit the chosen geometry of the vacuum chamber, whose relevant part of the realization is shown in **Figure 4**. The chamber is realized with commercial 10 inch ConFlat flanges for the vertical body assembly, which will host both pendulums. Two thin steel tubes were welded across it to provide tunnels for the passage of the movable field mass system. These tubes are 100 mm in diameter and cannot therefore host cylinders greater than say 90 mm in diameter, together with their cradle which will be necessary for their management.

While the expression of Eq. (7) is valid for one pendulum in the "near" configuration, the effect on the other pendulum of field masses in that position must also be studied because it

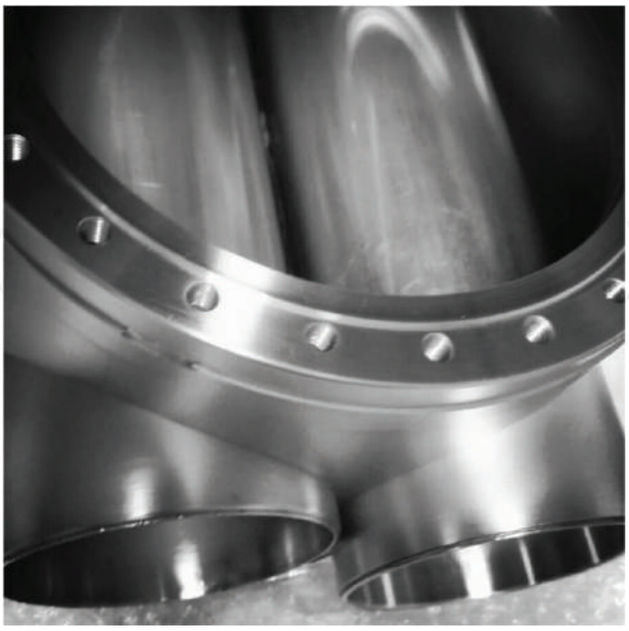

Figure 4. Detail of the lower chamber of the UHV vacuum system, showing the two thin steel tubes that allow management of field masses without feedthroughs by keeping them outside the vacuum vessel.

gives raise to the relative frequency change y_{far} of the "far" configuration which appears in Eq. (4). As a matter of fact, this effect is not so small, given the fact that the two pendulums are contained in the same vacuum vessel of **Figure 4**.

In order to facilitate this calculation, while increasing the signal by a factor of two, the idea was conceived to design the field mass system as a periodic structure. In fact, it can easily be shown that increasing w, the length of the field mass cylinders, would cause a signal reduction which would take the signal to vanish if the length is taken to infinity. This happens because such a structure would produce no field gradient in the longitudinal direction. Only a modulation along x of the mass density can produce a field gradient. The periodic structure which is planned, with a density switch between ρ_M and zero (or the lower density of another material) for every length of 2 w, will produce a periodic field gradient along x which vanishes at the center of all regions of uniform density. A pendulum centered at such vanishing gradient points will experience an increased frequency when positioned in correspondence with the higher density material and a symmetrically decreased frequency when positioned in correspondence with the lower density one.

By placing the two pendulums inside the vacuum vessel at a distance 2 w from each other, within a periodic field mass system so conceived, as shown in **Figure 5**, the measured DROC will be doubled because while one pendulum is pulled up, the other one is pulled down. The opposite will then happen after the whole field mass system is displaced by 2 w to invert the centering of the two pendulums.

In practice, an infinite length of the field mass system cannot obviously be deployed, and the structure must be truncated at some point. In **Figure 6**, a calculation is shown of the expected relative gravitational extra acceleration in the case of a nine-mass-long truncated periodic structure. The material of field masses was assumed to be tungsten, dimensions were the same of **Figure 3**, and the density of air in between masses was neglected.

Details of acceleration uniformity around the rest point are given in **Figure 7** for both positions of the two pendulums, at the center of the middle field masses (upper curve) and at the center of the first air gap at their right (lower curve). It can be noticed that the latter is asymmetric. This is because the truncated periodic structure is asymmetric with respect to that point, with five masses on one side and only four on the other one. However, the effect on frequency of such asymmetry is expected to vanish to first order, as long as the rest point of the pendulum is correctly centered. In any case, centering of the pendulums will be important for accuracy as much as uniformity of the extra acceleration. Nevertheless, it can be noticed that a subtraction of the slanting baseline in the lower curve will make it appear very similar

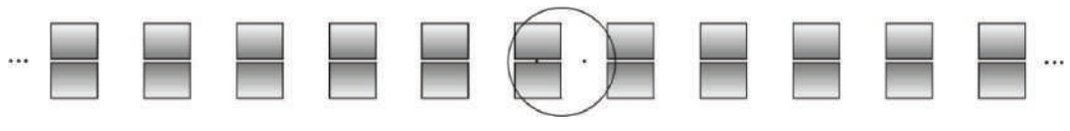

Figure 5. Scheme of the periodic field mass principle. Rest positions of the two bobs are shown (black dots). The circle in the middle represents the outline of the lower vacuum chamber through whose tunnels, shown in **Figure 4**, the field mass systems go.

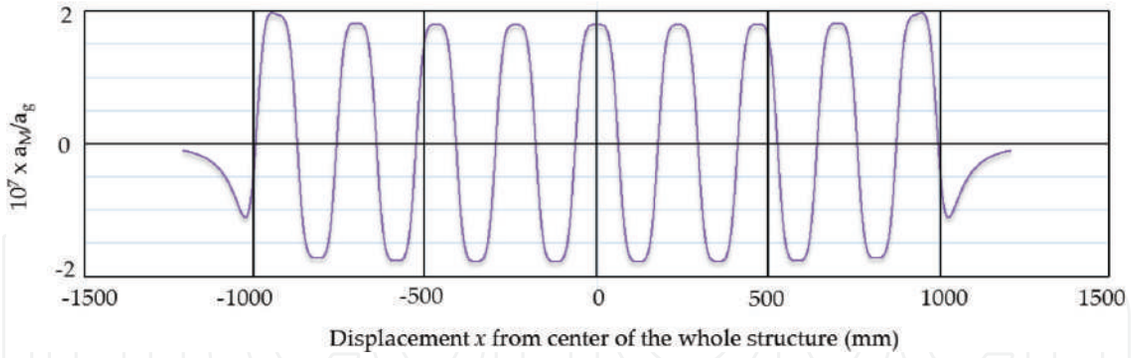

Figure 6. Calculated relative extra acceleration for a pendulum positioned at x from the center of a periodic field mass structure truncated to nine masses.

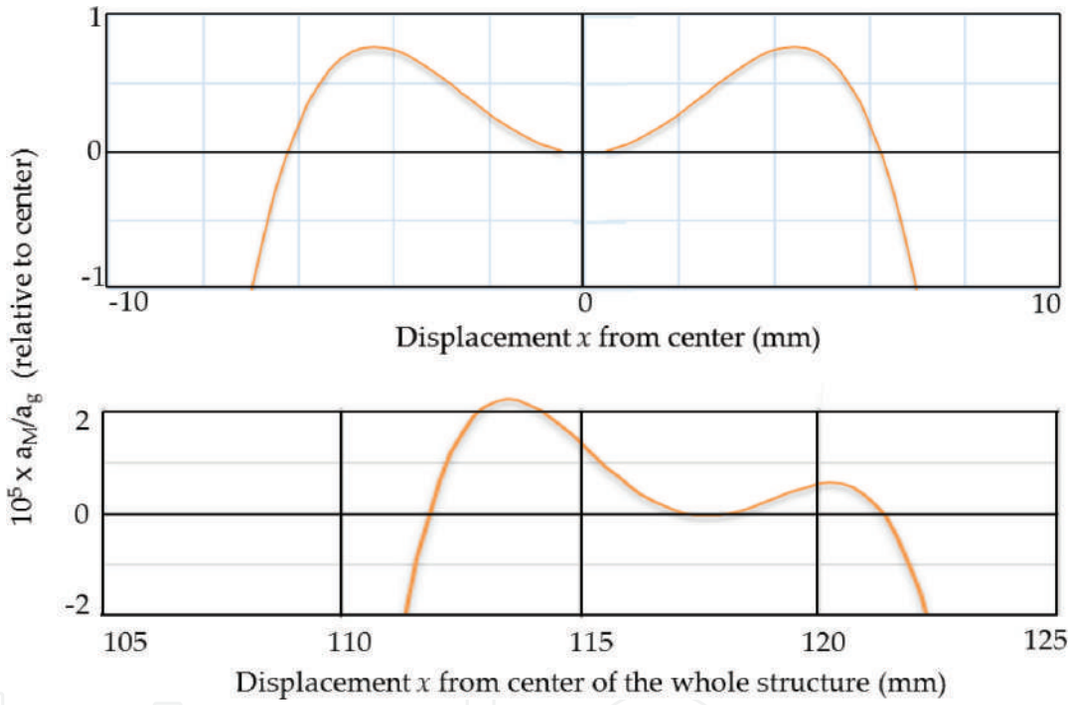

Figure 7. Relative uniformity of the extra acceleration for a pendulum positioned at the center of the middle masses (upper display) and one positioned at the center of the first gap (lower display), as a function of x, distance from the center of a nine-mass-long periodic structure. Uniformity was optimized here by trimming $\eta = w/a$.

to the upper curve for what concerns uniformity. Since both remain within +/− 10^{-5} up to 7 mm either side of the center, integration of the extra gravitational effect will be straightforward for peak pendulum oscillation amplitudes up to 7 mm if the target accuracy is at the 10^{-5} level.

In any case, all geometrical characteristics of the field mass system affect the proportionality constant K of Eq. (4), including the uniformity of their mass density and their stability in operational environmental conditions (like temperature expansion or deformation under mechanical stress). Adequate care must then be taken in design, realization, and handling of the field mass system.

To be truthful, in this respect, the experiment presented here is no different from any other experiment that was or will be tried to measure G. Revisiting the geometry of the field mass system for accuracy optimization will then be necessary after the concept is proven, which

http://dx.doi.org/10.5772/intechopen.75635

is the real target of the present work. Such an operation will most likely belong to a national metrology institute and not to a university. What this effort wants to prove is that no real obstacle exists in this approach on the way to an accuracy of 10^{-5}, other than problems that may come from accuracy and stability of the field mass system.

More benign is the requirement on positioning of the bob's trajectory with respect to active masses. In fact, it turns out that both in the horizontal and vertical direction, the extra acceleration features an extreme versus trajectory positioning, as shown in **Figures 8** and **9**, respectively: a minimum in the center for the lateral direction and a maximum a little above masses' gravity centers for the vertical.

The vertical displacement of the maximum is due to the extra vertical pull down that field masses exert if they are moved lower than the bob, which adds to Earth's gravity and hence to recall force, until they get too far down to be relevant. Such maximum is $(a^2 + w^2)/3\,L$ above the masses' gravity centers, which turns out to be almost 3 mm for the assumed masses. The

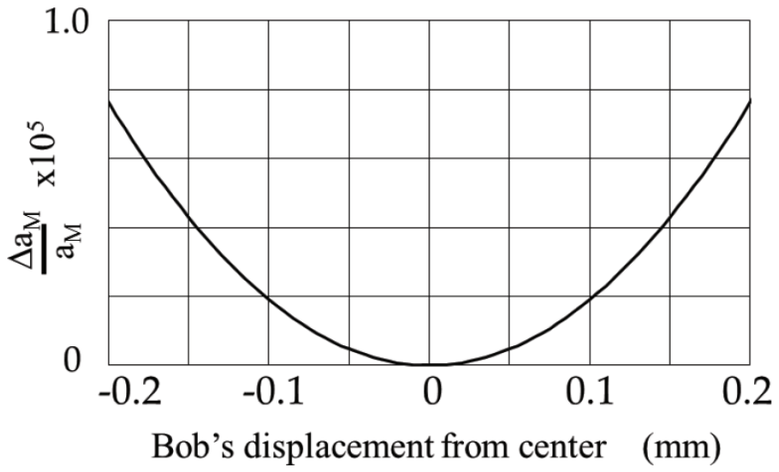

Figure 8. Relative variation of extra pull for lateral displacement of the bob's trajectory from the symmetry plane between field masses.

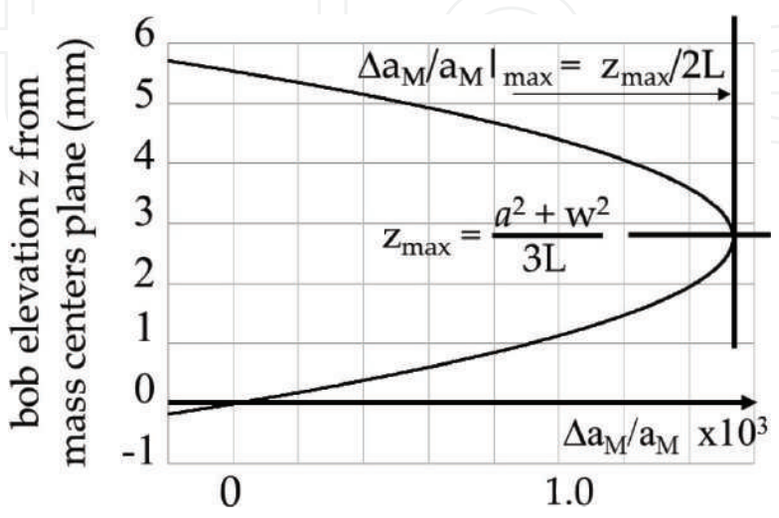

Figure 9. Relative variation of the relevant effect for vertical displacements of the bob's trajectory from the plane of mass centers.

relative shift is below $7 \cdot 10^{-4}$, which must be evaluated only to 1% for an accuracy contribution well below 10^{-5}, and the vertical positioning tolerance is 0.2 mm either side of the maximum, just like that of transverse horizontal positioning.

4. Pendulum design and optimization

The pendulums to be used in the experiment should be designed with the double target in mind of maximizing both accuracy and differential stability.

For accuracy, they should be "ideal," meaning that in their behavior they should not differ from the description that can be made with a mathematical model, supported by an adequate experimental characterization, in a way that can make G measurements uncertain by more than the desired accuracy. To this aim, all non-idealities affecting differential measurements between the two configurations of the field mass system should be considered. The main problem in this respect seems to be the uncertainty in the position of the center of mass of the pendulum given by the nonvanishing mass of the suspension relative to the bob. This shifts high the effective center of mass in a different way for the attraction of the Earth and that of the field mass system.

For differential frequency stability, which should exceed 10^{-12} for a full repetition period T_R, three main characteristics should be optimized in design and realization. They are:

1. Environmental sensitivity, especially versus temperature
2. Amplitude-to-frequency conversion, which induces frequency variations if the oscillation amplitude is not constant
3. Quality factor Q of the resonator, which is relevant in two ways: to obtain a long time constant in case of free decay operation [1] and to maximize stability with a given S/N ratio in case of sustained oscillations

Stability against environmental changes may be particularly critical for temperature, if not addressed, because at least a few ppm per Kelvin must be assumed for the linear expansion coefficient of the suspension, unless some kind of compensation is made. This is a quite common practice in pendulum clocks, but the demand in this application is severe. Even in the case of a successful compensation by a factor of ten of a low-expansion suspension material (e.g., tungsten, with its 4.3 ppm/K), the requirement would still be for a temperature differential between the two pendulums of the order of a few K for the necessary 10^{-12} differential frequency stability. It is true that the two pendulums are contained in the same vacuum vessel, which can be temperature stabilized, but an excellent thermalization scheme must certainly be devised for the purpose. It is assumed here that gold plating of the inner surface of the vacuum vessel or if necessary cylindrical gold-plated mirrors focusing the two suspensions [14] onto each other are the best bet to this aim, but a detailed discussion of the problem is out of the scope of this paper. What instead can be done at the pendulum design phase is implementation of a temperature compensation scheme. To this aim, tungsten is used for the suspension of the bob, and aluminum is deployed in an expansion compensation structure as shown below.

http://dx.doi.org/10.5772/intechopen.75635

Amplitude-to-frequency (or period) conversion is a well-known problem of pendulum clocks, because period-to-period instability of the kick turns into frequency instability through such connection, and famous in this perspective is the solution proposed by Christiaan Huygens in his 1657 patent of making an initial ribbon section of the suspension wrap on cycloidal profiles each side as it swings back and forth. However, neither Salomon Coster (who built the first such device, still shown in Boerhaave Museum in Leiden) nor anyone later appeared to be able to take full advantage of Huygens' idea, presumably because realizing a faithfully cycloidal profile is very difficult, as its curvature diverges in the cusp, where the shape is most important for small oscillations, which is where pendulum clocks are operated for wear minimization and consequent long-term stability.

In the model chosen for this experiment, pictured in **Figure 10a** with the bob in between field masses, the pendulum suspensions are made of tungsten wires hanging between two cylinders on which they wrap and unwrap. The wires are two for each pendulum, converging on the bob, for removal of the degeneracy of the two orthogonal modes, and the wire section above the cylinders is dimensioned for temperature compensation in a scheme that includes an aluminum structure to fix the length of the upper part of the wires.

Cylinders are technologically very easy to fabricate, contrary to the cycloidal case, and very good ones are common in modern machines, which makes them easy to obtain and cheap. In this work, dowel pins and specifically wrist pins are employed. The latter are very well rectified and have a hard surface because they must bear high forces with little friction in connecting pistons to rods in ICE power trains. As for amplitude-to-frequency conversion, deploying circular profiles does not realize a completely isochronous pendulum like Huygens showed true for a cycloidal profile; nevertheless, they produce a period vs. amplitude curve which shows a minimum at a certain amplitude value which is related to the diameter *D* of the cylinders. For that magic amplitude, the pendulum is then locally isochronous, and operation exactly at that amplitude shows no amplitude-to-frequency conversion. This means that the effect on frequency of amplitude variations vanishes if the amplitude is set correctly and that it depends quadratically on the amplitude error from that magic value in a way that makes it possible to achieve the necessary stability.

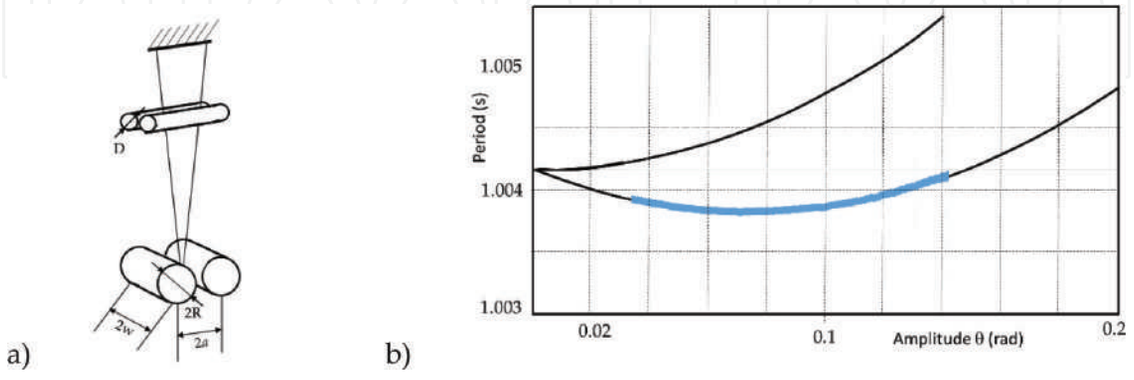

Figure 10. (a) Picture of the pendulum configuration chosen for this work, with the bob hanging between field masses, and (b) period versus amplitude curve of such pendulum compared to the one of a mathematical pendulum. Length is about 250 mm and D is 22 mm. The experimental points are superimposed on the measured section of the curve.

The period versus amplitude curve is compared to that of a mathematical pendulum in **Figure 10b**. The shape is still parabolic, but the vertex is moved from the vanishing amplitude point to an amplitude which can be chosen and adapted to the desired pendulum energy by suitably designing *D*, as shown in [15]. Period measurements, compared to the theory in **Figure 10b**, were taken on a 0.25-m-long pendulum with cylinders of 22 mm in diameter.

In fact, since at the apex of the parabola the two curves of **Figure 10b** show the same curvature, their local description is well known to be

$$\frac{\Delta T}{T_{min}} = \frac{1}{16}(\Delta\theta)^2 \tag{8}$$

which means that amplitude deviations $\Delta\theta$ from the minimum period spot must not exceed 4 μ rad to keep the first term at the 10^{-12} level. On the other hand, a period-to-period amplitude reduction is unavoidable due to energy loss and is related to it by

$$\frac{\Delta E}{E_{min}} = 2\frac{\Delta\theta}{\theta_{min}} = \frac{2\pi}{Q} \tag{9}$$

which means that the minimum pendulum quality factor Q_m necessary to keep the amplitude from decreasing more than the acceptable limit $\Delta\theta$ in one period is

$$Q_m > \pi\frac{\theta_{min}}{\Delta\theta} \tag{10}$$

For example, if θ_{min} = 0.075 rad, as in the case of **Figure 10b**, the quality factor must be greater than about 10^4 to keep the period (and the frequency) within 10^{-12} for one period, and a *Q* of 10^7 will keep the desired frequency stability for less than an hour at most. Luckily, because it's only the differential frequency stability that must be very stable, this requirement applies only to the difference of the two pendulum quality factors, provided they are both oscillating at the sweet amplitude spot. If it can be assumed that both quality factors are the same within say 10%, a *Q* of 10^7 would be enough to guarantee that the desired differential stability is kept for a full working day. This would be a long enough time for two full cycles of the repetition rate of the experiment if the system of field masses is kept in one position for a couple of hours and then moved to the other position for another couple of hours. Such is the situation for an experiment based on a pair of pendulums operated in free decay mode, and it could possibly be improved more if the two quality factors are within 1% of each other, in which case the experiment could go on for almost a week. Modeling out the effect may also be possible to some extent, as silently assumed in [1], and might further increase the useful duration of the experiment between periodic operations of amplitude reset, but this gets more complicated.

Alternatively, at the light of the experimented difficulty in obtaining consistently the extremely high *Q* values which are needed for the discussed reasons if the free decay mode must be adopted, a sustained oscillation approach can be tried for the two pendulums. In this perspective, a synchronous forcing term must be applied to the pendulum, designed to exactly recover the energy lost by friction. The best for stability and most efficient way of doing this would be a sine-wave force *F* applied in phase with the velocity *u* of the bob. This approach

avoids pulse timing and duration problems often encountered in the past by pendulum clock makers. The amplitude of such forcing term can be regulated in closed loop, by an automatic gain control (AGC) arrangement, to exactly compensate the dissipated power P_d at the desired swing amplitude. This requires the average delivered mechanical power $< Fu >$ to be

$$< Fu >= P_d = \frac{\omega \mathbf{e}}{Q}. \tag{11}$$

Since the energy **e** stored in the pendulum swing is proportional to the amplitude squared and u is linear with amplitude, it appears that the desired force is proportional to amplitude, as it might be intuitively expected. However, this is true only if Q is constant with amplitude, which turns out not to be the case for the adopted pendulum design. An analysis of what were felt to be the two main dissipation mechanisms for this structure was given in [1] and showed that in both cases the Q limitation is proportional to some power κ of the amplitude. In detail, periodic stretching of the wires under varying tension and their bending as they wrap and unwrap on the cylinders produce Q limitations which are inversely proportional to the square of the amplitude for the former ($Q_s \propto \theta^{-2}$, where s stands for stretching) and proportional to the amplitude's three-halves power for the latter ($Q_b \propto \theta^{3/2}$, where b stands for bending). Within that simplified theory, cyclic length variations of wires were overlooked, and only stretching under varying tension and bending on the cylinders were analyzed for small oscillations. Expressions obtained for the corresponding Q limitations (Q_s and Q_b, respectively) were

$$\frac{Q_s}{Q_f} = \frac{16}{9\sqrt{\varepsilon_0}\theta^2} \tag{12}$$

$$\frac{Q_b}{Q_f} = \left(\frac{LD}{\phi^2}\varepsilon_0\theta\right)^{3/2}, \tag{13}$$

which shows that $\kappa_s = -2$ and $\kappa_b = 3/2$. Here ε_0 is the static strain imposed on wires by the weight of the bob, ϕ is the wires' diameter, and Q_f is the intrinsic Q of the wire material. The total Q of the pendulum can then be obtained as

$$\frac{1}{Q} = \frac{P_{ds}+P_{db}}{\omega E} = \frac{1}{Q_s} + \frac{1}{Q_b}, \tag{14}$$

and features a maximum Q value at an angular swing amplitude θ_{max} which can both be calculated from Eqs. (12) through (14).

An example of such a Q dependence on amplitude is given in **Figure 11a** as calculated from Eq. (14) for a pendulum which could be suitable for the G experiment (L = 1 m and D = 4 mm), built with 4 μm Tungsten wires and a spherical 4.5 mm tungsten bob. The resulting peak force that is necessary to keep the bob swinging at the given amplitude according to Eq. (11) is shown in **Figure 11b**, where the strange effect appears that, in the branch before the minimum, weaker forcing terms are needed to maintain greater amplitudes.

A comprehensive campaign to confirm the theory in all conditions has not been completed yet as this book is going in press. In particular, Q values in excess of several millions were

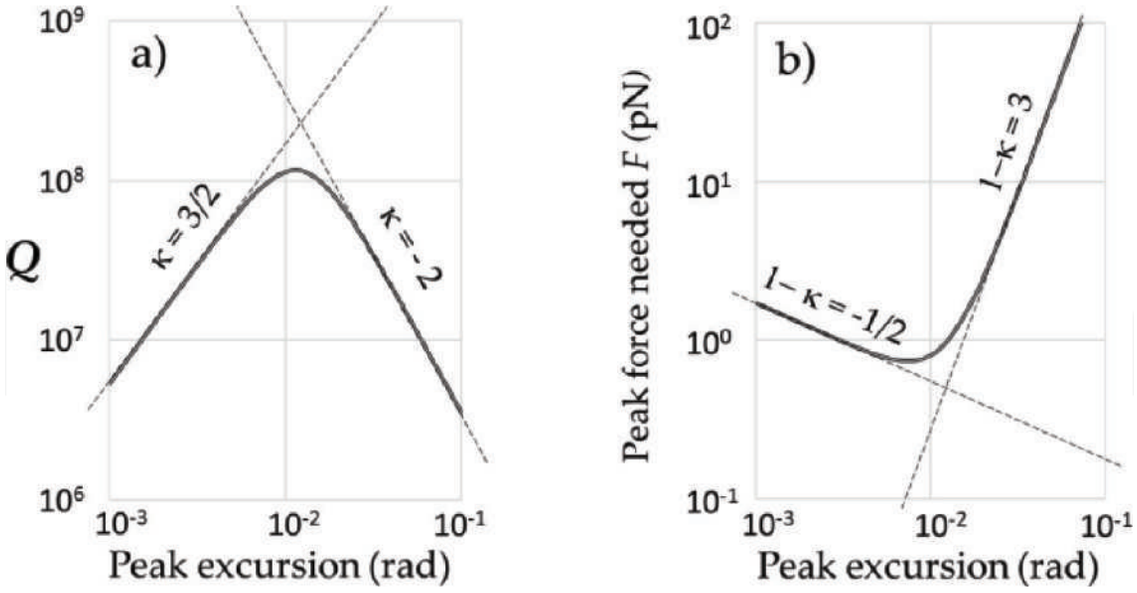

Figure 11. (a) Q as a function of angular oscillation amplitude and (b) peak force value of the sinusoidal forcing term necessary to maintain the corresponding amplitude, calculated for a pendulum with 4-mm-diameter suspending cylinders and 1 m length, made with 4 μm Tungsten wires and a spherical 4.5 mm tungsten bob.

not observed yet in the limited range of configurations that were staged, which suggests that there may be other dissipation mechanisms worth studying, but it seems unlikely that a more complete analysis may not confirm the general shape of these curves. In fact, experimental results obtained by analyzing free decay ringdown amplitude data clearly show that such *Q* maximum exists. Further experiments are in progress, as well as the analysis of such additional dissipative phenomena as belt friction, squeeze film energy loss [16], and more trivially dissipation in the structure holding the experimental arrangement.

What must be underlined here is that, due to the *Q* behavior shown in **Figure 11**, Eq. (11) points to a criticality for AGC stability, because amplitude stabilization cannot be reached if increasing the amplitude requires a reduction of the forcing term. The derivative of the required force with respect to amplitude must be positive for AGC stability, which imposes the selection of a swing amplitude in a region where the dominant dissipation mechanism is such that $\kappa < 1$. If $\kappa > 1$ the AGC will be unstable, and if $\kappa = 1$ it will not be effective because the necessary force does not depend on amplitude. Conversely, given a desired swing amplitude, as dictated, for example, by the range of acceptable field uniformity of **Figure 7**, the design of pendulum suspensions should observe the specification of placing the desired amplitude in a range where AGC stability is guaranteed.

The best choice in this respect appears to be a design which positions the θ_{max} at the desired oscillation amplitude, which is what was tried in the simulation of **Figure 11**, where the amplitude of maximum *Q* was made to correspond at 10 mm with a bob peak excursion which can be judged desirable from the calculated effect uniformity shown in **Figure 7**. However, it must be pointed out here that this design problem is still open because also the minimum of the period, as illustrated in **Figure 8**, must be placed by design at the same oscillation amplitude, which implies a tight restriction on the acceptable values of *D*, the diameter of suspension

cylinders. These values are much smaller than the one adopted in the simulation of **Figure 11** to force the position of the Q maximum. Clearly, full confirmation of the Q theory must be carried out before the pendulum design can be finalized.

Another detail which is obviously relevant to this effect is the material of the suspension wires, because both Q_f and ε_0 in Eqs. (12) and (13) are material dependent, as well as the diameter ϕ of the wires, in its own way. Unfortunately, mechanical characterization of fibers is less than complete in the open literature, particularly for what concerns mechanical losses summarized by Q_f. Therefore, tests were carried out in the laboratory with a purposely built apparatus [17] on promising candidates, mainly aiming at characterization of mechanical losses, creep, and linearity [18]. Para-aramid, SiC, basaltic, and carbon fibers were analyzed [19], as well as steel and tungsten metal wires. Glass and fused quartz are still waiting in line. No doubt, a final decision on this important item must be integrated with the whole design of the pendulum, as both analyzed loss mechanisms depend on ε_0, and hence on ϕ, while the bending loss, in particular, depends also explicitly on ϕ.

Three more very important items must be considered in the design of the pendulum because they have an impact on the operation of the device, if not on its effectiveness in detecting the gravitational field modulation. They are the mode map of the pendulum, the oscillation detection system, and the excitation mechanism in case of forced oscillations' operation mode.

The first one may affect obtainable Q values and introduce fastidious coherent noise in the detection signal. In fact, if undesired oscillation modes get excited, albeit weakly, they can easily increase the effective total damping by sucking energy into dissipative mechanisms which do not belong to the main pendulum mode, lowering its Q as a consequence, and on the other hand, they force detection data processing to face spurious coherent signals which may reduce S/N ratio and ultimately affect resolution. Getting rid of spurious signals is impossible by the Nyquist theorem because of aliasing if the sampling frequency is not at least double the highest undesired mode frequency, which forces the handling of a massive amount of data in a full sine-wave detection system. The most difficult undesired modes to deal with, however, are the ones that are closest in frequency to the pendulum mode [20], because they are the ones that are most easily excited. In particular, the transverse mode, whose degeneracy with the pendulum mode is removed by the double-wire suspension structure, remains close to it in frequency if the angle between wires is not too big.

Other modes that should be focused on are the double pendulum mode and the similar balance wheel mode, which are more separated in frequency but are easily excited as soon as some imperfection appears in the suspension structure or in the excitation system, if present.

Given the boundary conditions emerging from the panorama spelled out here, care must be taken in designing and realizing excitation and detection systems for the two pendulums, to minimize the risk of getting undesired modes excited and affecting in this way damping and measurement resolution. Both optical and electromagnetic methods have been analyzed for both. All tested methods have their own advantages and problems, but all can serve the purpose if well implemented.

5. Attitude control

One final problem must be addressed here to give a complete picture of the complexity of this apparently very simple experiment: the attitude of the whole apparatus with respect to the vertical direction, as defined by the Earth's local gravity vector, can affect the operation of pendulums and must therefore be guaranteed to be adequately accurate and stable in time, if necessary by active attitude control. Two different problems must be addressed in this respect as both the absolute tilt and its stability are relevant, in different ways.

The absolute verticality is important because the two cylinders must be guaranteed to be horizontal for the symmetry of the swing, which in turn guarantees the positioning of the minimum period in amplitude space (the curve of **Figure 10** was calculated for the case of two cylinders at the same level). Because the pendulums are two, this issue is complicated by the need to have both pairs of suspension cylinders aligned on the same horizontal plane.

The attitude stability is particularly critical in the case of low sampling-rate detection, like simple flyby time stamping at half periods, because of the heavy aliasing of seismic angular noise [1] that it produces. In **Figure 12**, a series of background seismic power spectrums is reported, as collected in different locations of the global seismographic network [21]. A peak at about 0.2 Hz appears in all of them, which is produced by low damping surface Rayleigh waves excited by ocean waves hammering the shores, extended with reduced intensity at higher frequencies. Because of their low frequency, it is very difficult to filter out such seismic angular noise contributions.

Work done to attack this problem includes passive and active attitude control [22, 23]. However, passive filtering was quickly understood to be inadequate for the purpose, not only because of its awkwardness at such low frequencies but also because of the need for stiffness of the structure holding pendulums to prevent detrimental effects of recoil from pendulums on attitude stability and damping itself. Active stabilization was then decided to be necessary, and work

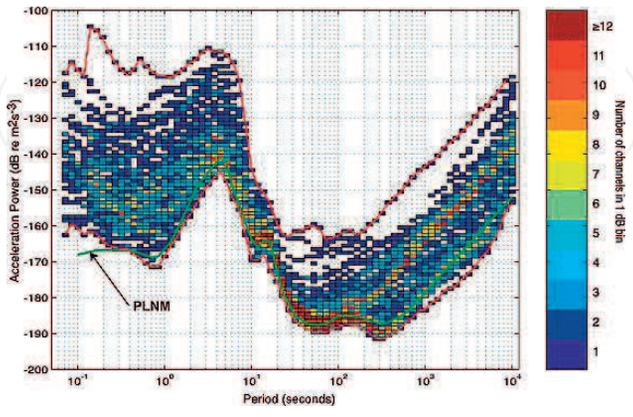

Figure 12. Background seismic power spectrums, as collected in different locations of the global seismographic network. High noise at periods above 1s (i.e. Fourier frequencies below 1 Hz) is caused by far travelling Rayleigh surface-waves excited by ocean waves.

was done to realize for the purpose a high-sensitivity tiltmeter [24] with sub-nanoradian resolution and special half-pole actuators based on thermoelectric devices [25]. The problem of substantial angular stability improvement by active control is not trivial because a tiltmeter with the necessary sensitivity was never seen with resonance-limited bandwidth above, say, 10 Hz, which provides not much more than a decade range in the Fourier frequency domain for open-loop gain increase from the zero-dB level of the loop bandwidth allowed by a typical 45° phase margin to the desired open-loop gain at the seismic peak sub-Hertz frequency. The half-pole actuator was developed for this reason, so that a loop-gain roll-off of 30 dB/dec could be achieved without resorting to a digital control, allowing in this way a guaranteed-stability servo operation with low-frequency open-loop gain in excess of 40 dB.

Nevertheless, the seismic angular noise problem is expected to be much more benign in case of acquisition of the whole sine-wave swing signal at a conveniently high sampling rate. For this reason, and because acquisition of the full sine wave is necessary anyway for oscillation support, unless the free ringdown approach is adopted, the choice was made to develop a suitable detection method for this purpose. The latter can be electromagnetic, based on the generation of an e.m.f. in a wire swinging through a magnetic field together with the suspenders of the bob, or optical, based on a linear position-sensitive detector deployed to translate the bob's position in an electrical signal.

The first approach has the advantage of measuring the bob's velocity, with which the forcing term should be in phase, and is therefore to be preferred for phase accuracy of the oscillation loop but implies the risk of introducing in the experiment undesired electromagnetic forces which could be greater than the weak gravitational force that must be measured.

The second approach, on the contrary, is less risky of introducing undesired forces but requires the generation of a sine-wave signal in quadrature with the detected position for the implementation of the forcing term. This must be performed very accurately to obtain oscillations at exactly the resonance frequency because any error from quadrature would introduce a frequency shift, which in turn may build an error on G if it's not adequately common moded between the two pendulums.

Similar considerations hold for the forcing sine wave, which can be realized with just a current-carrying wire attached to the suspenders in a voice coil type of device in the first approach and if Q is high enough could be implemented by radiation pressure in the second.

6. Accuracy budget

A tentative accuracy budget for the experiment described here is given in [1]. Because of the highly efficient time and frequency metrology approach, only geometrical uncertainties are expected to be relevant at the level of 10^{-5}, provided the necessary differential stability of 10^{-12} can be achieved. This is clearly a big "if," as discussed above, because it assumes that seismic and mode leakage problems are adequately solved. However, it can be in principle obtained if the limitation is electronic noise. It must be noted here for completeness that the

Effect	Relative bias	Uncertainty	Conditions
Shift at bob's vertical position	$6.7 \cdot 10^{-4}$	$<10^{-6}$	< 50 μm uncertainty in *a*, w
Bob's vertical position	0	$2 \cdot 10^{-6}$	0.2 mm full tolerance
Bob's lateral position	0	$1.7 \cdot 10^{-6}$	0.2 mm full tolerance
Non-isochronism	$-1.8 \cdot 10^{-5}$	$< 10^{-7}$	Operation at minimum period
Spacing between twin masses	0	$6 \cdot 10^{-6}$	0.4 μm gap uncertainty
Field masses' dimensions	0	$6 \cdot 10^{-6}$	1 μm uncertainty
Field masses' density	0	$5 \cdot 10^{-6}$	

Table 1. Accuracy budget projection based on 1-m-long 4 μm tungsten fibres, 6-mm-diameter suspension cylindrical profiles, a swing amplitude of 0.01 rad, and a 5 mm tungsten bob. The position of field masses' gravity center is assumed known with <300 nm uncertainty.

best pendulum clocks ever realized [13] were probably not differentially stable better than 10^{-9} at the target 10^4 s averaging time, which means that 60 dB improvement is necessary. Although this is granted on paper by projected S/N and *Q*, actually achieving it is still a big challenge. On the positive side, it is worth pointing out here that energy-induced amplitude changes [11] do not affect frequency if operation is kept at the minimum period isochronous point and that an approach to oscillation support aimed at overcoming pulse stability problems by moving to a sine-wave excitation system similar to that employed in high-stability quartz oscillators will remove one of the worst contributions to instability.

This said, it can be seen in **Table 1** that most geometrical contributions to uncertainty impose quite loose requirements at the target accuracy level of 10^{-5}, with the sole exception of size and positioning of field masses, which must be guaranteed at high accuracy. While other contributions enjoy relaxed specifications granted by parabolic minima which are specific of this configuration, the latter do not and must comply with specs which are similar to any other big G experiment. However, the expectation that accuracy on G may be limited by control on this single geometry contribution ushers the possibility of doing even better than 10^{-5} if resources were to become available to improve the accuracy of field masses. A summary of such uncertainties is reported in **Table 1**, as listed in Ref. [1], where the reader can find more details and a deeper discussion on accuracy.

7. Conclusions

A new experiment was presented for the determination of the Newtonian constant. It is based on a time and frequency metrology approach consisting in the measurement of the small frequency difference between two freely oscillating pendulums via their time delay rate of change. A system of dense field masses is moved back and forth between the two, alternately increasing one frequency and reducing the other and vice versa. The increase in resolution by averaging is fast in this case because the limiting noise is white delay noise, which yields $\sigma_y(\tau)$

proportional to $\tau^{-3/2}$. This fact is unique among experiments for the determination of G and offsets the poor signal size problem allowing to focus the design on accuracy rather than S/N ratio. It remains to be shown that differential stability in the 10^{-12} region can be obtained with consistency for two similar pendulums of the design which has been sketched here. This seems to be a long shot when considering the absolute stability achieved by the best Shortt clock [13], because it requires an improvement of more than three orders of magnitude with respect to it, at the target few hours (T_R) averaging time. However, it is not unreasonable to think that two adequately similar pendulums can be realized, and if they are within 100 mm of each other, it can be expected that g uniformity may be adequately stable in time to support the assumption. A description of the apparatus and a discussion of pendulum design optimization for this experiment were offered in detail, pointing out problems and possible solutions. Work is in progress on the preparation of the experiment, considering both a free decay solution and pendulum operation with active support of oscillations and amplitude control. It is expected that an accuracy of 10^{-5} may be obtained for G with the proposed approach, limited only by the accuracy of field masses' size and positioning, and that it may be possible in a metrology laboratory to reduce limiting geometrical uncertainties enough to push it into the 10^{-6} range.

Acknowledgements

The author wishes to thank for encouragement and discussions Robert Drullinger, Stephan Schlamminger, and Bill Phillips of NIST and Valter Giaretto, Mario Lavella, and Lamberto Rondoni of the Politecnico di Torino. Special thanks go to Luca Maffioli for his master's thesis on the pendulum analysis and to Meccanica Mori of Parma for the TIG welding of the thin steel tubes to the experimental chamber. The author also wishes to acknowledge the support of the US Department of Commerce and NIST through the Precision Measurements Grant Program, Award ID number 70NANB15H348.

Author details

Andrea De Marchi

Address all correspondence to: andrea.demarchi@polito.it

Department of Electronics and Telecommunications, Politecnico di Torino, Torino, Italy

References

[1] De Marchi A. A frequency metrology approach to Newtonian constant G determination using a pair of extremely high Q simple pendulums in free decay. Journal of Physics: Conference Series. 2016. DOI: 10.1088/1742-6596/723/012046

[2] Rothleitner C, Schlamminger S. Measurements of the Newtonian constant of gravitation, *G*. Review of Scientific Instruments; **88**(11):111101. DOI: 10.1063/1.4994619

[3] Quinn T, Speake C, Richman S, Davis R, Picard A. A new determination of *G* using two methods. Physical Review Letters. 2001;**87**:111101

[4] Schlamminger S, Holzschuh E, Kundig W, Nolting F, Pixley RE, Schurr J, Straumann U. Measurement of Newton's gravitational constant. Physical Review D. 2006;**74**:082001

[5] Parks HV, Faller JE. Simple pendulum determination of the gravitational constant. Physical Review Letters. 2010;**105**:110801

[6] Schwarz JP, Robertson DS, Niebauer TM, Faller JE. A free-fall determination of the Newtonian constant of gravity. Science. 1998;**282**:2230

[7] Fixler JB, Foster GT, McGuirk JM, Kasevich MA. Atom interferometer measurement of the Newtonian constant of gravity. Science. 2007;**315**:74

[8] Lamporesi G, Bertoldi A, Cacciapuoti L, Prevedelli M, Tino GM. Determination of the Newtonian gravitational constant using atom interferometry. Physical Review Letters. 2008;**100**:050801

[9] De Marchi A, Ortolano M, Berutto M, Periale F. Simple pendulum experiment for the determination of the gravitational constant G: Progress report. In: Proceedings of 6th Symposium on Frequency Standards and Metrology; September 10-14, 2001; Fife. 2002. p. 538

[10] Berutto M, Ortolano M, Mura A, Periale F, De Marchi A. Toward the determination of *G* with a simple pendulum. IEEE Transactions on Instrumentation and Measurement. 2007;**56**:249. DOI: 10.1109/TIM.2007.890785

[11] Berutto M, Ortolano M, De Marchi A. The period of a free-swinging pendulum in adiabatic and non-adiabatic gravitational potential variations. Metrologia. 2009;**46**:119

[12] Sullivan D, Allan D, Howe D, Walls FL. Characterization of Clocks and Oscillators. NIST Technical Note. Obtainable from NIST, US Department of Commerce. Vol. 1337. 1990

[13] Van Baak T. A Dream Pendulum Clock. 2009. leapsecond.com

[14] Giaretto V. Private Communication. 2008

[15] Maffioli L. Mathematical modelization and experimental validation of a simple pendulum for the measurement of the Newtonian constant *G* [Master Thesis]. Politecnico di Torino; 2013

[16] Schlamminger S, Hagedorn CA, Gundlach JH. Indirect evidence for Lévy walks in squeeze film damping. Physical Review D. 2010;**81**:123008

[17] Ceravolo R, De Marchi A, Pinotti E, Surace C, Zanotti Fragonara L. A new testing machine for the dynamic characterization of high strength low damping fiber materials. In: Experimental Mechanics. Vol. 57. New York: Springer LLC; 2016. p. 10. ISSN: 0014-4851. DOI: 10.1007/s11340-016-0208-4

[18] Zanotti Fragonara L, Pinotti E, Ceravolo R, Surace C, De Marchi A. Non-linearity detection and dynamic characterisation of aramid and silicon carbide fibres. International Journal of Lifecycle Performance Engineering. 2016;**2**:15. Interscience Publishers. ISSN: 2043-8656. DOI: 10.1504/IJLCPE.2016.082708

[19] Ceravolo R, De Marchi A, Pinotti E, Surace C, Zanotti Fragonara L. Measurement of weak non-linear response of Kevlar® fibre damaged by UV exposure. Composite Structures. Elsevier; 2017. p. 12. ISSN: 0263-8223. DOI: 10.1016/j.compstruct.2017.10.056

[20] Ortolano M: Misura della costante gravitazionale con pendolo in vuoto [PhD thesis]. Politecnico di Torino; 2001

[21] Berger J, Davis P, Ekstroem G. Ambient earth noise: A survey of the global seismographic network. Journal of Geophysical Research. 2004;**109**. DOI: B11307

[22] Berutto M. Isolamento da trumore meccanico di una piattafoma [PhD thesis] Politecnico di Torino; 2004

[23] Mura A. Measurement of the Newtonian gravitational constant with dynamic pendulum [PhD thesis]. Politecnico di Torino; 2009

[24] Berutto M, Ortolano M, Periale F, De Marchi A. Realization and metrological characterization of a compact high-resolution pendulum tiltmeter. IEEE Sensors Journal. 2005; **5**(1):26-31

[25] De Marchi A, Giaretto V. The elusive half-pole in the frequency domain transfer function of Peltier thermoelectric devices. Review of Scientific Instruments. 2011;**82**:034901. DOI: 10.1063/1.3558696